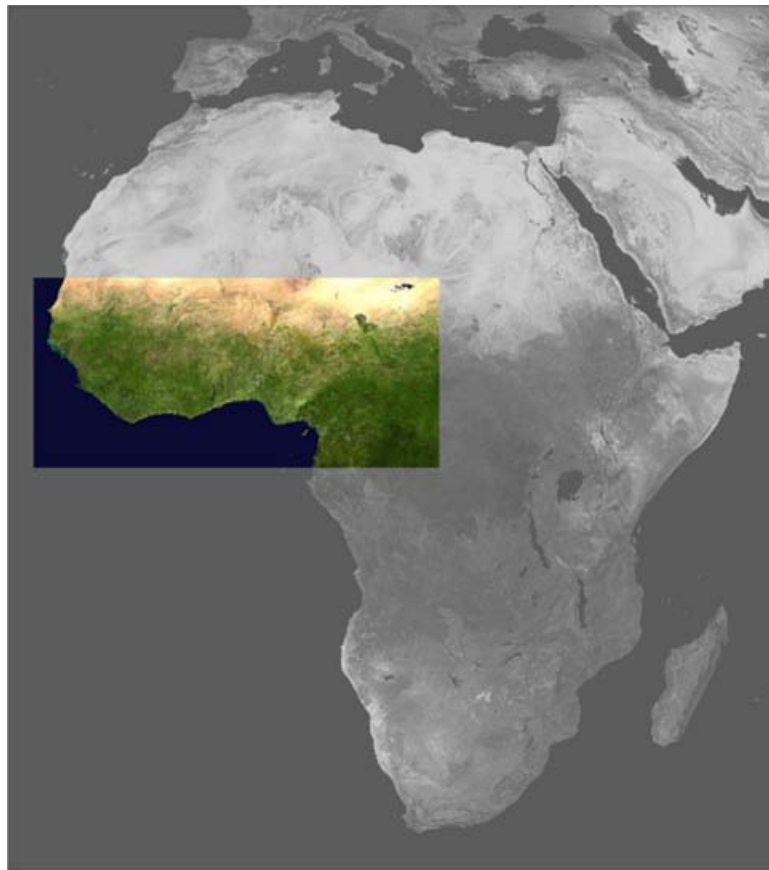


Scientific Report 15-01

High-resolution climate simulations for West Africa

Cathrine Fox Maule and Wilhelm May





Colophon

Serial title:

Scientific Report 15-01

Title:

High-resolution climate simulations for West Africa

Subtitle:

DMI-HIRHAM5 West Africa 12-km run

Authors:

Cathrine Fox Maule and Wilhelm May

Other Contributors:

-

Responsible Institution:

Danish Meteorological Institute

Language:

English

Keywords:

Africa, HIRHAM5

Url:

www.dmi.dk/dmi/sr15-01

ISSN:

1399-1949

ISBN:

978-87-7478-656-6 (online)

Version:

1

Website:

www.dmi.dk

Copyright:

Danish Meteorological Institute



Contents

Colophone	2
1 Introduction	4
1.1 Acknowledgements	4
2 The grid and domain of the RCM simulations	6
3 Evaluation; ERA-interim run	7
4 Historical simulations	15
5 Future scenario simulations	23
A Grid specifications	41

1. Introduction

As part of the ACCIC/Danida project, DMI is committed to conducting a series of high-resolution regional climate model simulations for West Africa (Activity 5.4), with the DMI-HIRHAM5 regional climate model. This report presents the results of these simulations. A total of eight simulations have been carried out, which are listed in Table 1.1 and described briefly below. The grid, domain and experimental setup for the simulations is presented in Chapter 2.

The HIRHAM5 model is a regional hydrostatic climate model developed by combining and adapting the dynamical core of the HIRLAM weather forecast model (Eerola, 2013) with the physical schemes of the ECHAM5 global circulation model (Roeckner *et al.*, 2003). The model employs a semi-Lagrangian time stepping scheme to improve computational performance.

To evaluate the performance of the DMI-HIRHAM5 regional climate model (Christensen *et al.*, 2006) over West Africa, one simulation of a so-called 'perfect boundary experiment' has been carried out. HIRHAM5 has been forced with ECMWF's re-analysis data, ERA-interim, and the output of HIRHAM5 is compared with observations of key meteorological parameters for the period 1989-2010. Based on this the performance of HIRHAM5 over the West African domain can be evaluated. This is presented in Chapter 3.

For the remaining simulations, HIRHAM5 has been forced by a Global Circulation Model (GCM). We have used the ICHEC-EC-EARTH, r3i1p1 (Hazeleger *et al.*, 2012). A historical simulation with this GCM-RCM combination has been carried out covering 1986-2005. The output of precipitation and 2-m air temperature of the historical simulation has been compared with observations for the period, which allows evaluating the bias of the combined GCM-RCM simulation. A series of other parameters from the historical simulations are also presented in Chapter 4.

A total of six simulations have been made for different future scenarios and time-slices. The two IPCC standard emission scenarios, the Radiative Concentration Pathways, RCP4.5 and RCP8.5 have both been simulated for three different future time-slices, 2016-2035, 2046-2065 and 2081-2100. The results of projected climate changes over West Africa from these simulations are presented in Chapter 5.

Type	boundary/GCM	Experiment	Time-slice
Evaluation	ERAINT	Evaluation	1989-2010
Historical	EC-EARTH	Historical	1986-2005
Scenario	EC-EARTH	RCP4.5	2016-2035
Scenario	EC-EARTH	RCP4.5	2046-2065
Scenario	EC-EARTH	RCP4.5	2081-2100
Scenario	EC-EARTH	RCP8.5	2016-2035
Scenario	EC-EARTH	RCP8.5	2046-2065
Scenario	EC-EARTH	RCP8.5	2081-2100

Table 1.1: List of the simulations carried out for the West African domain with the DMI-HIRHAM5 regional climate model.



1.1 Acknowledgements

This work was funded by Danida. We acknowledge the use of the GPCP combined precipitation data, which were developed and computed by the NASA/Goddard Space Flight Center's Laboratory for Atmospheres as a contribution to the GEWEX Global Precipitation Climatology Project.

2. The grid and domain of the RCM simulations

The wish was to make a high-resolution simulation over a large part of West Africa. We chose to use a horizontal resolution of 0.11 degrees (about 12km), corresponding to the resolution of the high-resolution Euro-CORDEX simulations, and a simple sub-division of the CORDEX Africa resolution of 0.44 degrees. We chose to place the grid points of the high-resolution grid such that every 16th point coincide with the grid points of the CORDEX AFR-44 grid. The computational cost of the high horizontal resolution constitutes a limiting factor on the size of the domain, so the West Africa domain used in this study spans from 18.04°W to 22.11°E, and from 0°N to 18.04°N, which amounts to 366 gridpoints in the east-west direction, and 165 gridpoints in the north-south direction; the grid specifications are listed in Appendix A. To account for edge effects the actual simulation was carried out on a grid with 10 additional gridpoints in each direction. Figure 2.1 shows a map of the domain with and without the relaxation zone and the locations of the grid points in Burkina Faso to give an impression of the resolution. In all the remaining maps presented in this report the relaxation zone is excluded. In all the simulations the atmosphere is divided into 31 vertical layers. To avoid spin-up effects all the HIRHAM5 runs include a one year spin-up prior to each time slice. The time-step used in the simulation is 150s; a relatively short time-step was necessary for the simulation to remain stable. Despite the short time-step several of the simulations experienced instabilities, which was handled by tuning the horizontal diffusion coefficient.

The output variables stored, the filenaming and the meta-data of the files follow the CORDEX specifications (Christensen *et al.*, 2013). Most variables have been stored every 3, 6 or 24 hours, but the two key parameters, 2-m air temperature and precipitation, have been stored hourly, which is at a higher temporal resolution than CORDEX standards. Post-processed files are available for daily data and monthly means upon request.

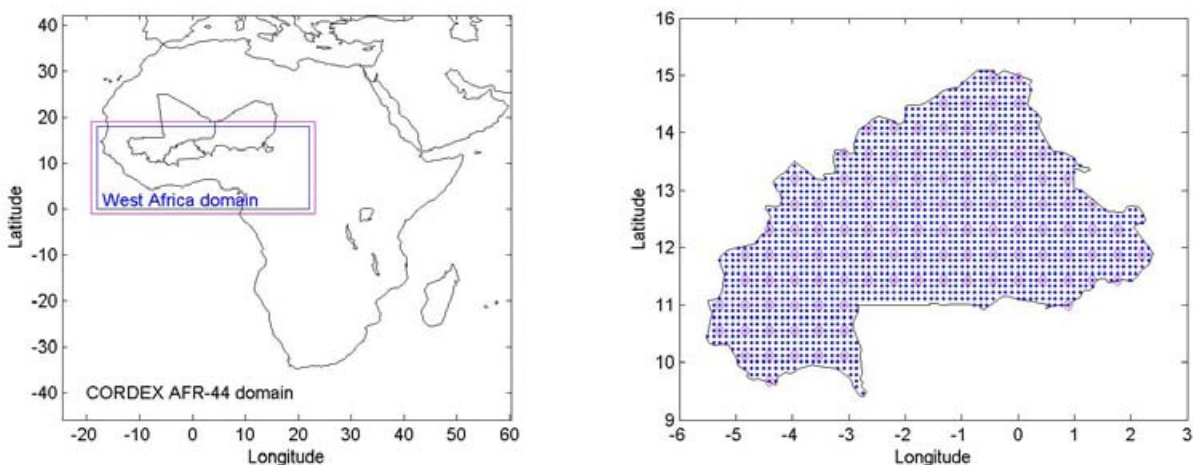


Figure 2.1: The map on the left shows the CORDEX AFR-44 domain (the whole map) and the West African domain (in blue) used in this study. The relaxation zone is shown in pink. To indicate the resolution of the simulations, the map on the right shows the locations of the individual grid points in Burkina Faso of the 0.11° grid used in this study (in blue) and of the CORDEX AFR-44 grid (in pink).

3. Evaluation; ERA-interim run

To evaluate the performance of HIRHAM5 over the West African domain, the RCM has been driven by ECMWF's ERA-interim re-analysis product (Uppala *et al.*, 2005; Dee *et al.*, 2011). This allows for comparison of the RCM's output with observed data as the weather of the RCM should resemble the actual weather of the period. The ERA-interim run spans the period 1989-2010.

For Africa it should be recalled that ground based data are sparse, which affects the quality of both the ERA-interim re-analysis data and the observational data. The observation data sets we have used includes the UDEL (University of Delaware) dataset (Legates & Willmott, 1990), which is available on <http://climate.geog.udel.edu/~climate/>. The UDEL data set, which includes both temperature and precipitation, is gauge-based and has a spatial resolution of 0.5° and a monthly temporal resolution. We use version 3.01 for temperature (Matsuura & Willmott, 2012a), and version 3.02 for precipitation (Matsuura & Willmott, 2012b). In addition we use the GPCP (Global Precipitation Climatology Project) data set, which is available on <http://www.esrl.noaa.gov/psd/data/gridded/data.gpcp.html>. It only includes precipitation, but combines gauge observations and satellite-based precipitation data.

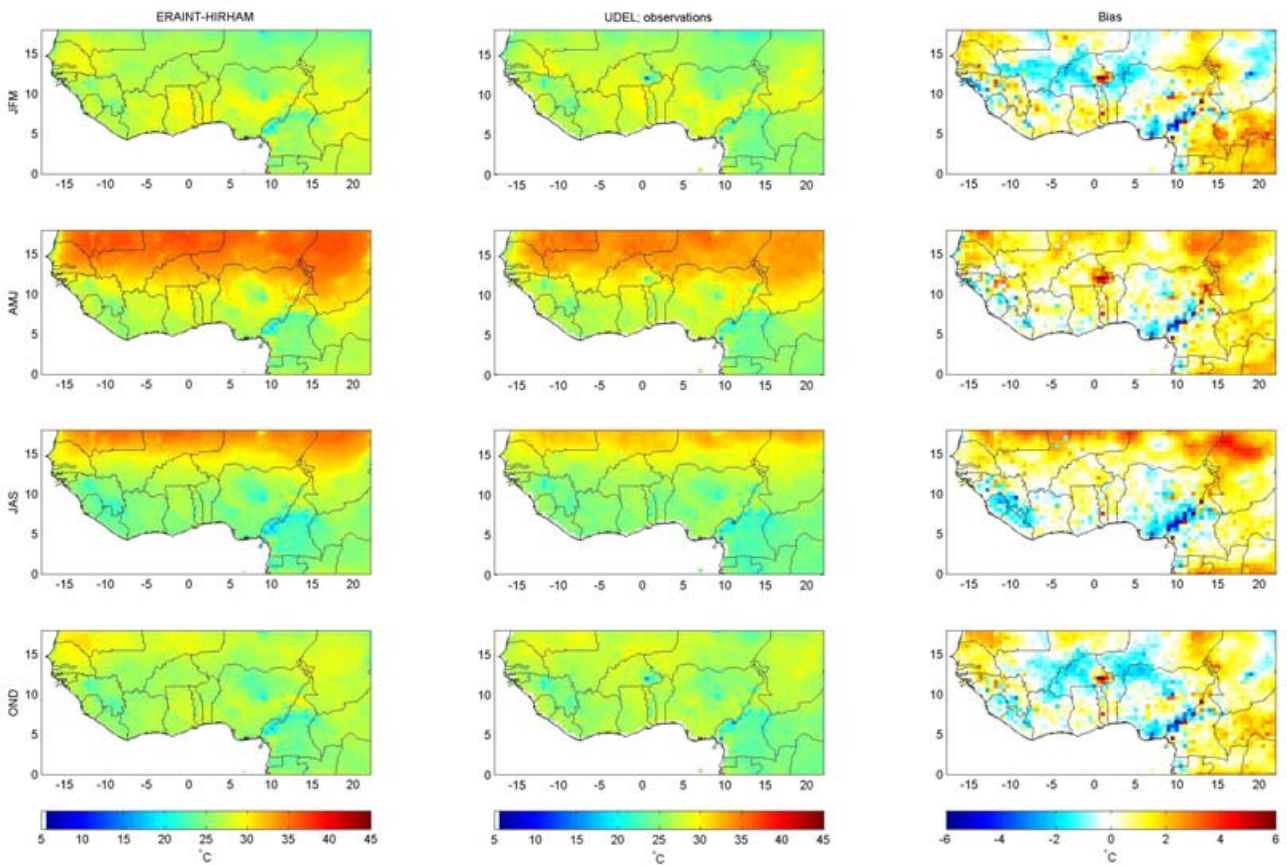


Figure 3.1: Left column shows the seasonal mean 2-m air temperature of ECMWF-ERAINT DMI-HIRHAM5 run from 1989-2010 for the four seasons; the middle column shows the seasonal means of the UDEL gridded observations and the right column shows the temperature bias for each season.

It has a spatial resolution of 2.5° and a monthly temporal resolution. We have chosen to use two different precipitation data sets for evaluating HIRHAM, as the observation data sets are known to differ (Nikulin *et al.*, 2012), due to the sparsity and low quality of observations in the region.

The maps shown are all divided into seasons. Dividing the year into four seasons of three months is not necessarily the most sensible way to separate seasons in this region of Africa. However, no obvious alternative exists which encompasses the entire region, as seasonality changes across the domain. Therefore we use January-February-March (JFM), April-May-June (AMJ), July-August-September (JAS) and October-November-December (OND) following Nikulin *et al.* (2012). The JAS season constitutes the core of the West African monsoon season.

Figure 3.1 shows the seasonal mean temperature of the ERAINT-HIRHAM5 simulation (left column) and of the UDEL gridded observation (middle column). The right column shows the temperature bias given as the model output minus the gridded observations. The bias is calculated by regridding the model output to the UDEL data's grid. To adjust for elevation differences a height correction of $0.006^\circ\text{C}/\text{m}$ has been applied. The figure shows that the bias is of the order of $+1^\circ\text{C}$ over a large part of the domain, with a higher warm bias in the eastern part of the domain. A strange feature is present in most seasons in the eastern

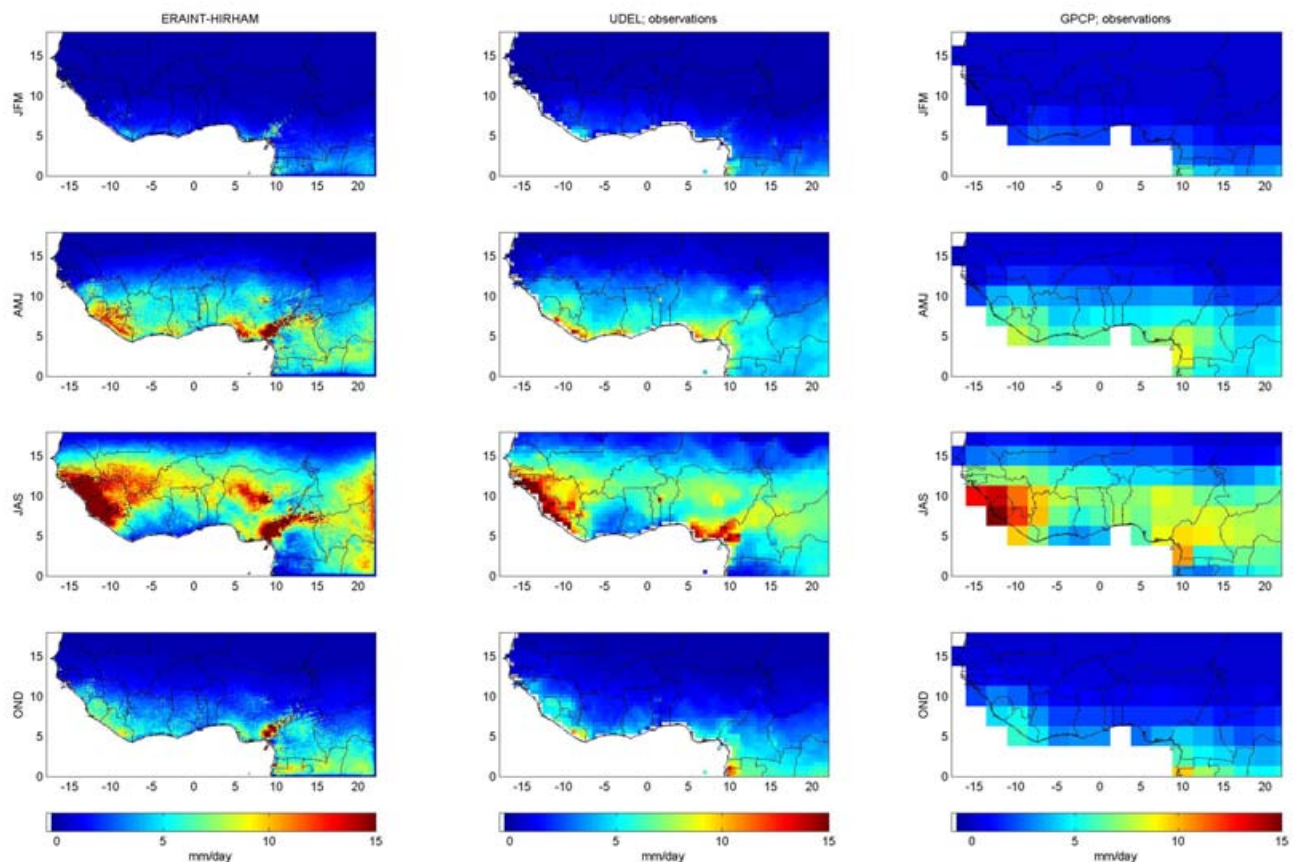


Figure 3.2: The left column shows the seasonal mean precipitation of ECMWF-ERAINT DMI-HIRHAM5 run from 1989-2010 for the four seasons, JFM, AMJ, JAS and OND from top to bottom. The middle column shows the seasonal mean precipitation from the UDEL gridded data in mm/day, and the right column from the GPCP data.

Burkina Faso, where the maps indicate a small area of strong warm bias. This relates to an area with low values of the UDEL gridded data.

Figure 3.2 shows the seasonal mean precipitation of the ERAINT-HIRHAM5 (left column), the UDEL gridded data (middle column) and the GPCP gridded data (right column) in mm/day. The different resolutions of the three data sets are evident. Figure 3.3 shows the bias of the seasonal mean precipitation in both mm/day and in % with respect to the UDEL dataset. The figure shows that HIRHAM5 generally has a wet bias in the southern part of the domain and a dry bias in the northern. Note that the relative precipitation bias is smallest in the rainy season (JAS). The seasonality of the precipitation is better illustrated in figure 3.4, where the monthly mean precipitation for three different subregions are shown. The figure shows that HIRHAM captures the seasonality of the precipitation fairly well, although it

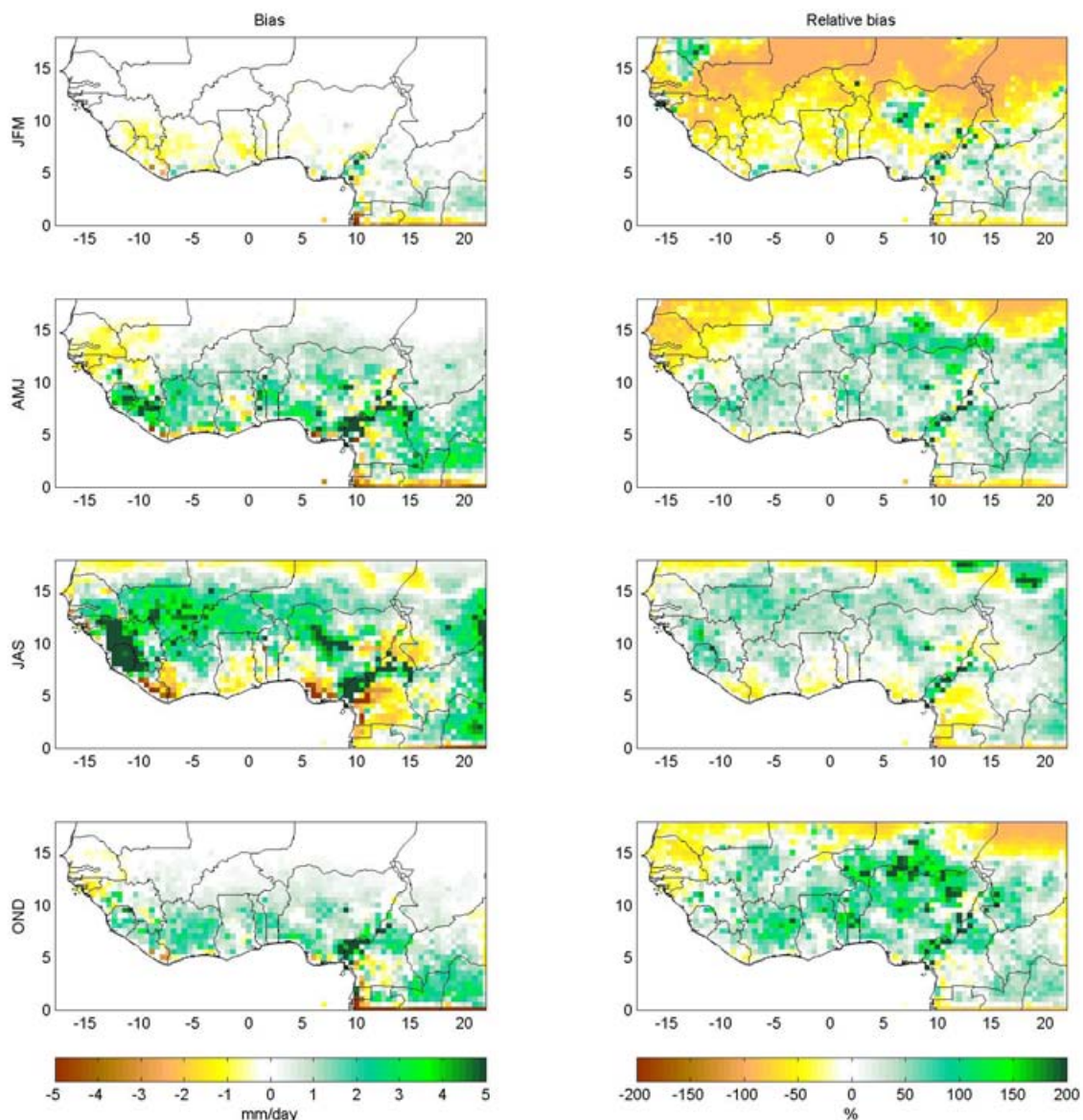


Figure 3.3: Bias of the seasonal mean precipitation of ECMWF-ERAINT DMI-HIRHAM5 run from 1989-2010 for the four seasons, JFM, AMJ, JAS and OND from top to bottom; left column is in mm/day, right column is in % compared to the observed.

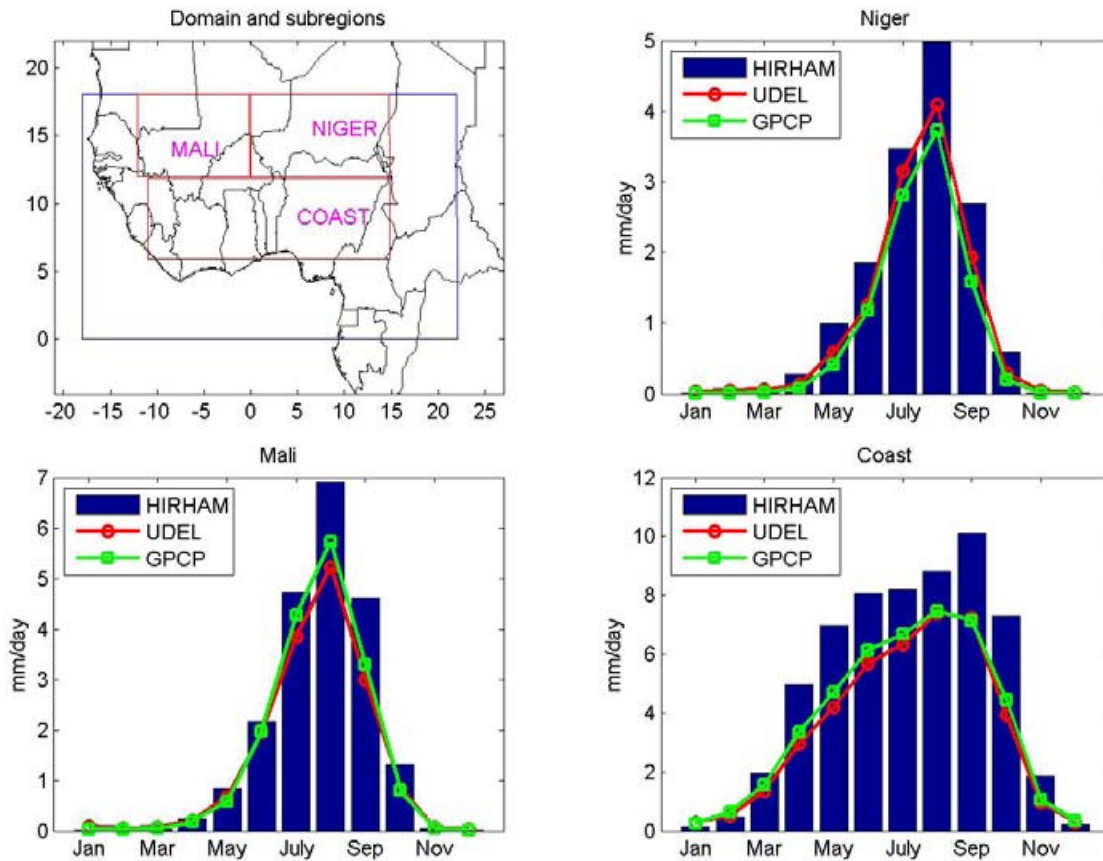


Figure 3.4: Monthly mean precipitation for three different subregions, one centered over Niger, one centered over Mali and one along the coast; the map in the upper left shows the three subregions (in red) and the entire domain (in blue). All values are means over regions and time (1989-2010). The monthly mean precipitation of HIRHAM5 is here compared to both UDEL and GPCP data.

overestimates the precipitation amount.

Figure 3.5 shows the seasonal mean evaporation in mm/day, the total runoff in mm/day and the total soil moisture content in kg/m². The total runoff clearly follows the pattern of the precipitation as expected. The latter displays only minor seasonal variability. Figure 3.6 shows the specific humidity, the surface wind speed at 10m in m/s and the surface downwelling short wave radiation in W/m².

Figure 3.7 shows the albedo used in HIRHAM5 as well as the observed black-sky albedo from CMSAF data from Deutscher Wetterdienst (DWD), and the bias of the albedo. The albedo of HIRHAM5 is too low in most of the domain in all seasons. A wrong albedo lead to a wrong radiation balance at the surface. A too low albedo means that too little radiation is reflected leading to an additional warming of the surface. This may be the cause of the warm bias that is seen in Figure 3.1.

To illustrate the transport of moisture across the domain, the seasonal means of the horizontal moisture flux ($q \cdot \vec{v}$) at 850hPa, is shown in Figure 3.8. From this figure it is quite evident that in both OND and JFM most moisture transport occurs from the continent towards the ocean, and in the two other seasons, the flow is reversed.

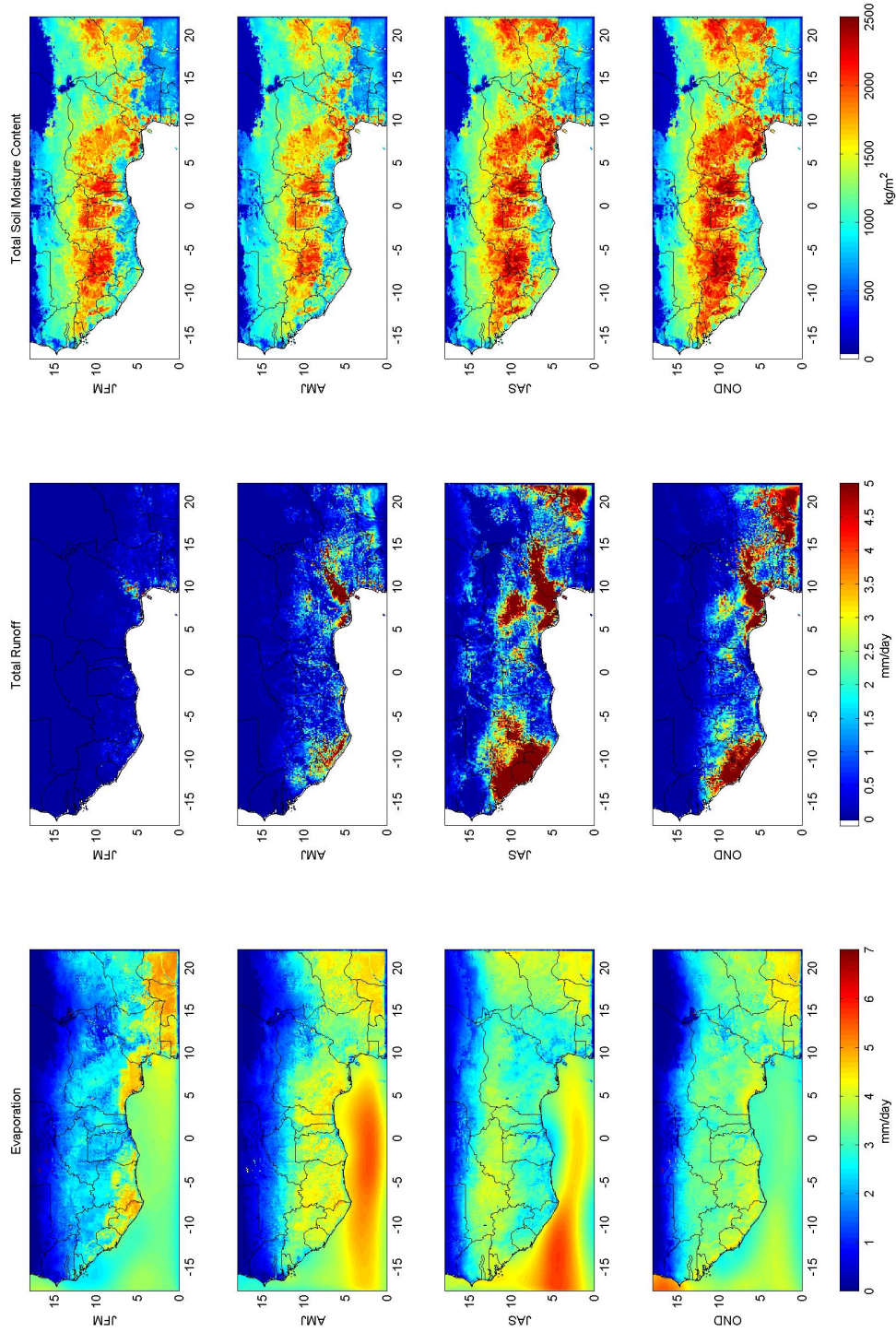


Figure 3.5: Left column shows the seasonal mean evaporation in mm/day of ECMWF-ERAINT DMI-HIRHAM5 run from 1989-2010 for the four seasons; the middle column shows the seasonal mean total runoff in mm/day and the right column shows seasonal mean total soil moisture content in kg/m².

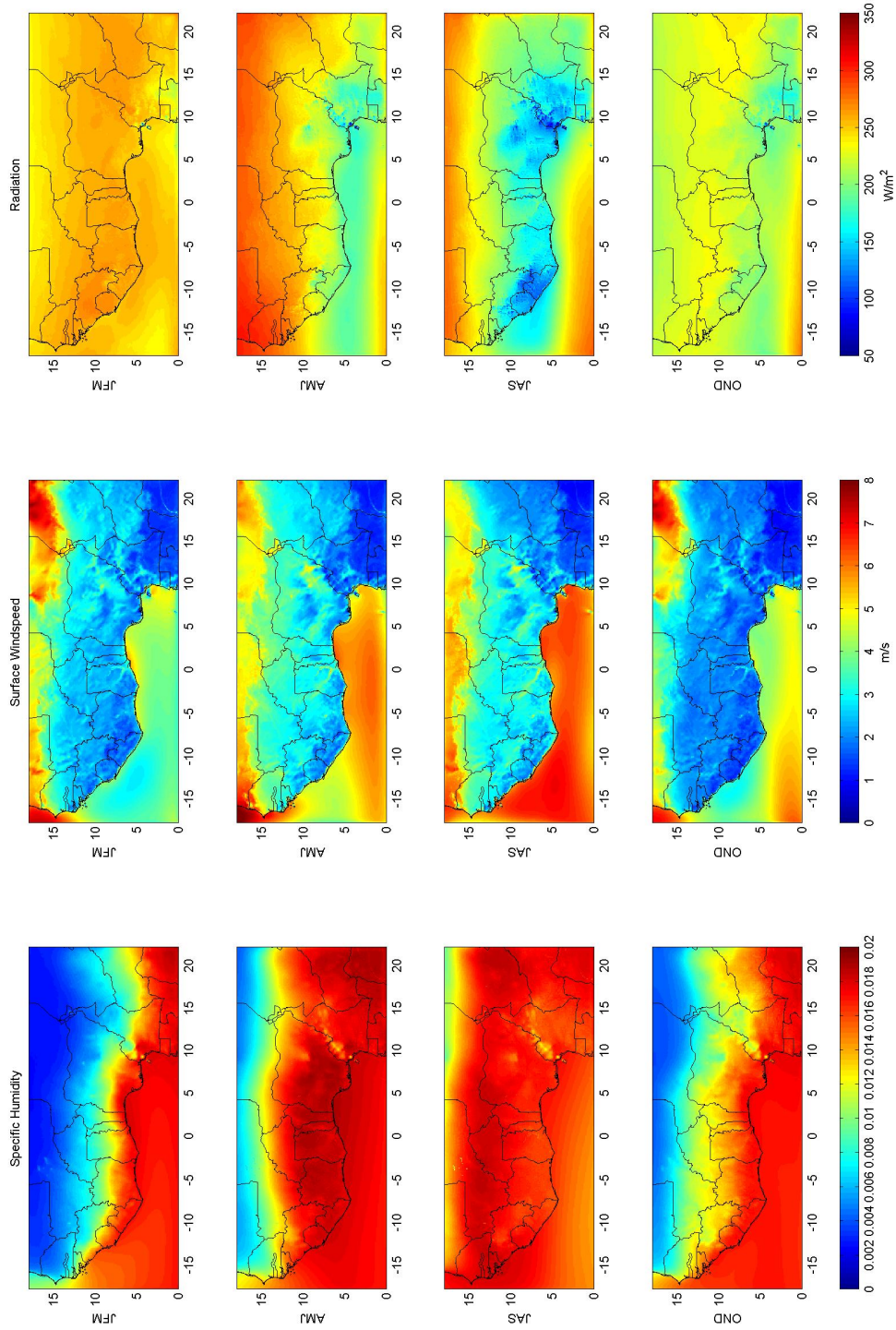


Figure 3.6: Left column shows the seasonal mean specific humidity of ECMWF-ERAINT DMI-HIRHAM5 run from 1989-2010 for the four seasons; the middle column shows the seasonal mean 10-m surface wind speed in m/s and the right column shows seasonal mean of the surface downwelling short wave radiation in W/m^2 .

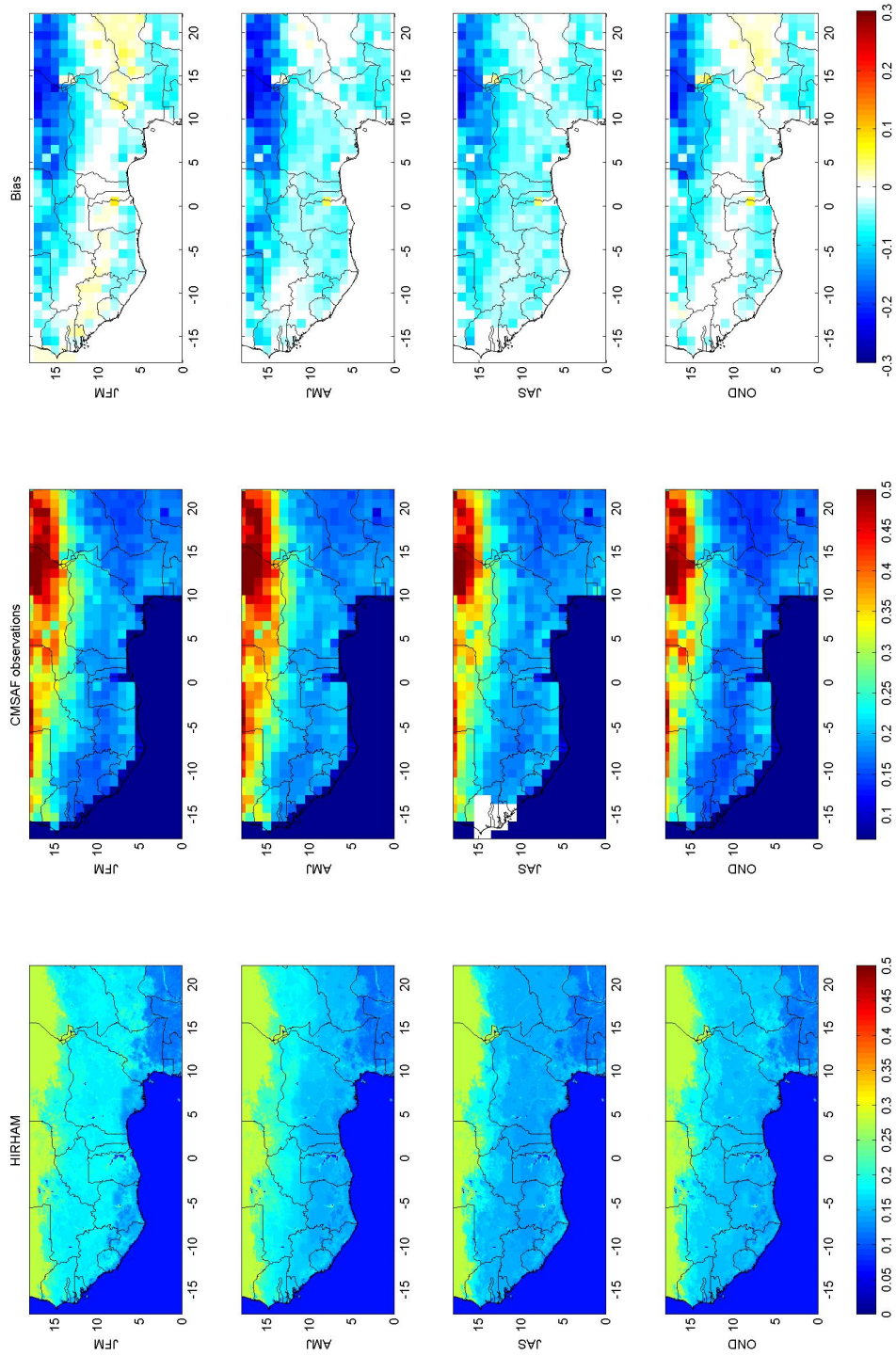


Figure 3.7: Left column shows the seasonal mean albedo of DMI-HIRHAM5 from 2008-2010 for the four seasons; the middle column shows the seasonal mean observed albedo from CMSAF and the right column shows seasonal mean bias of the albedo. The albedo of HIRHAM5 is too low in most of the domain in all seasons.

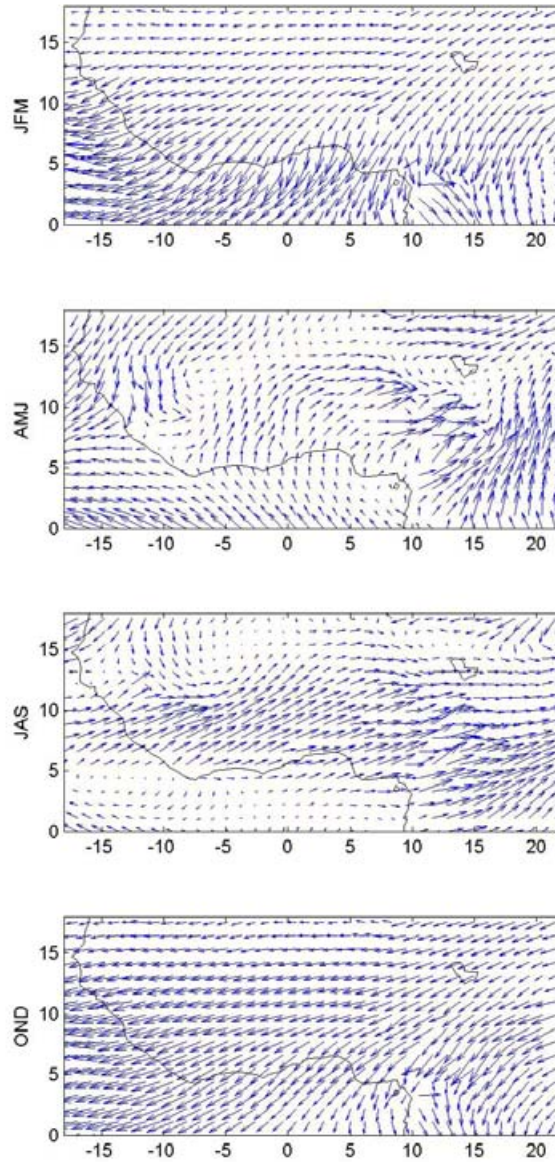


Figure 3.8: The figure shows seasonal means of the horizontal moisture flux, $q \cdot \vec{v}$, at 850hPa from ERA-Interim for 1989-2010.

4. Historical simulations

In this chapter we present some results of the historical simulation where HIRHAM5 has been driven by EC-EARTH for 1986-2005. In Figure 4.1 the seasonal mean 2-m air temperature of EC-EARTH, of the downscaled EC-EARTH-HIRHAM5 output, and of the gridded observations from UDEL are shown. This allows us to see the added value of the dynamical downscaling. The Figure shows that EC-EARTH has a strong cold bias over the region, but that HIRHAM5 mitigates part of this approaching the observed temperatures. It seems clear that the HIRHAM output gives a better representation of the observed temperatures in the region than EC-EARTH. Figure 4.2 shows the seasonal mean of the daily maximum and minimum temperatures, for reference the daily mean temperatures have been plotted again on the same scale as tasmax and tasmin.

In Figure 4.3 the temperature bias compared to the UDEL data set is shown. We find that the EC-EARTH-HIRHAM simulation has a strong cold bias in all seasons everywhere in the domain. The bias is smallest in JAS of about -1°C , in the other three seasons the bias is about -2°C to -4°C in the central parts of the domain, including Burkina Faso, Mali and

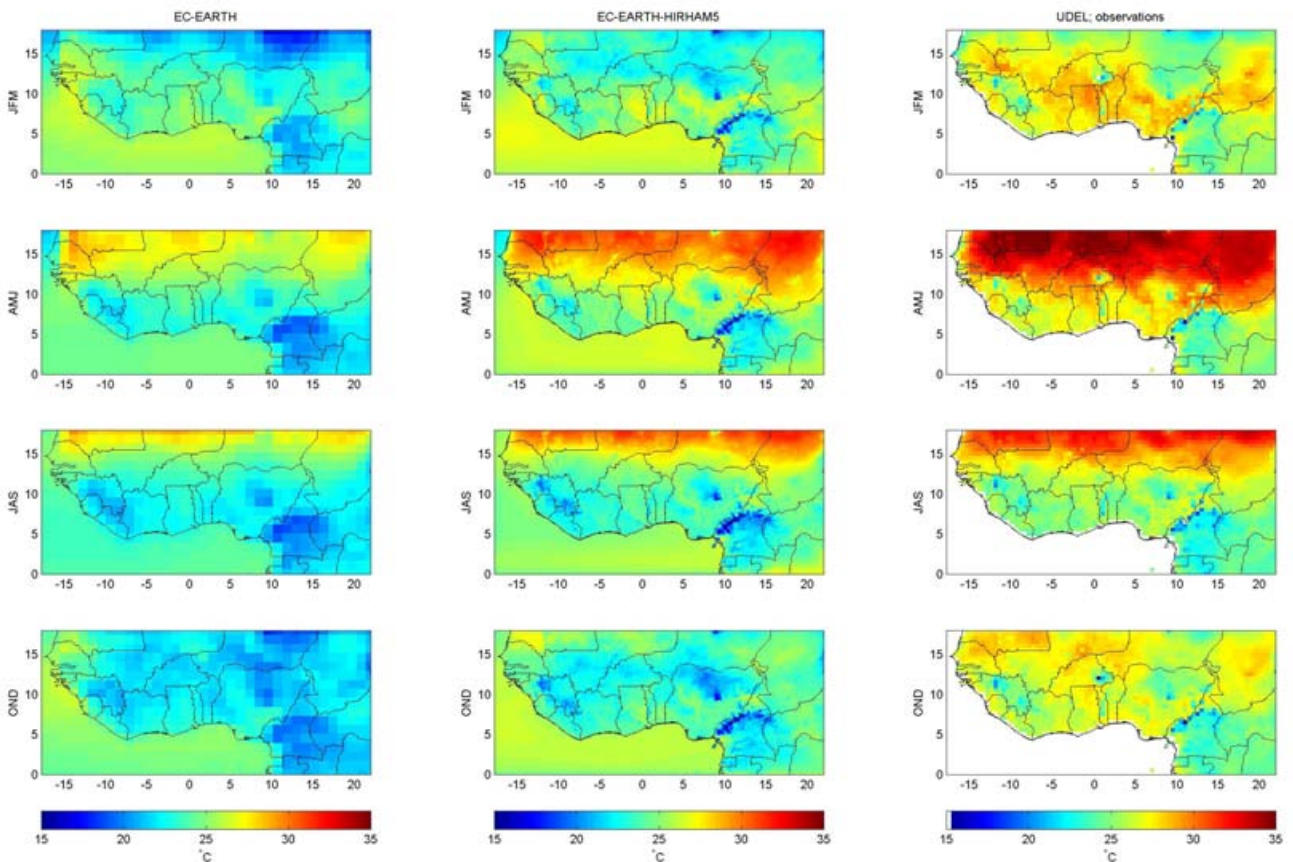


Figure 4.1: Comparing the 2-m air temperature of the EC-EARTH simulation (left), the downscaled EC-EARTH-HIRHAM5 simulation (center) and the UDEL observations (right) for the historical time-slice 1986-2005. UDEL observations are only available over land. The resolution of EC-EARTH simulation is approximately 125 km, the HIRHAM5 simulation about 12 km and UDEL about 55 km.

eastern Niger.

Figure 4.4 shows the seasonal mean precipitation of the historical simulation, and the precipitation bias compared to the UDEL data set. We find that EC-EARTH-HIRHAM has a wet bias in most of the domain in all seasons apart from JFM. Particularly in JAS, overlapping with the rainy season, the bias is large in southern Mali. Figure 4.5 shows the monthly precipitation for three subregions in the domain compared to both UDEL and GPCP observations. These figures underline the wet bias of EC-EARTH-HIRHAM and also demonstrate that particularly in the Mali-box and the Coast-box the bias is fairly evenly distributed over the rainy months. Concluding on both temperature and precipitation, the general picture is that EC-EARTH-HIRHAM is too cold and wet in West Africa in the historical period.

Figure 4.6 shows the seasonal mean evaporation (mm/day), the total runoff (mm/day) and the seasonal mean soil moisture content (kg/m²). Figure 4.7 shows the specific humidity, the surface wind speed (m/s) at 10m and the shortwave downwelling radiation at the surface (W/m²).

Figure 4.8 shows the horizontal moisture flux at 850hPa. Comparing this for the EC-EARTH driven historical simulation with the ERAINT-driven simulation shown in Figure 3.8, there

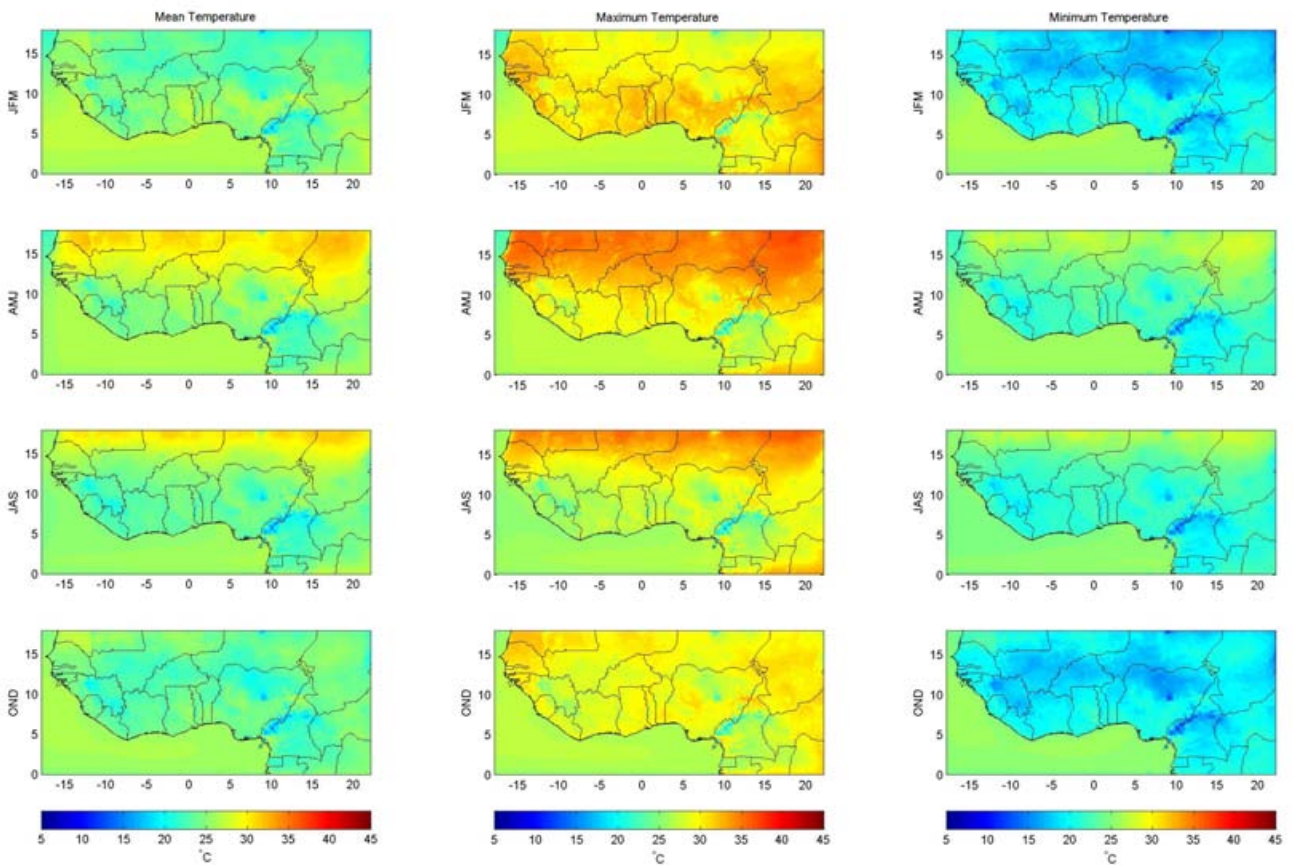


Figure 4.2: Left column shows the seasonal mean 2-m air temperature of EC-EARTH-HIRHAM5 historical simulation from 1986-2005 for the four seasons; the middle column shows the seasonal means of the daily maximum temperature and the right column of the daily minimum temperature.

are quite some differences. Particularly in AMJ the wind in the Gulf of Guinea is primarily southerly in the ERAINT driven simulation, while it is southeasterly in the EC-EARTH driven simulation. There are also noticeable differences in JAS.

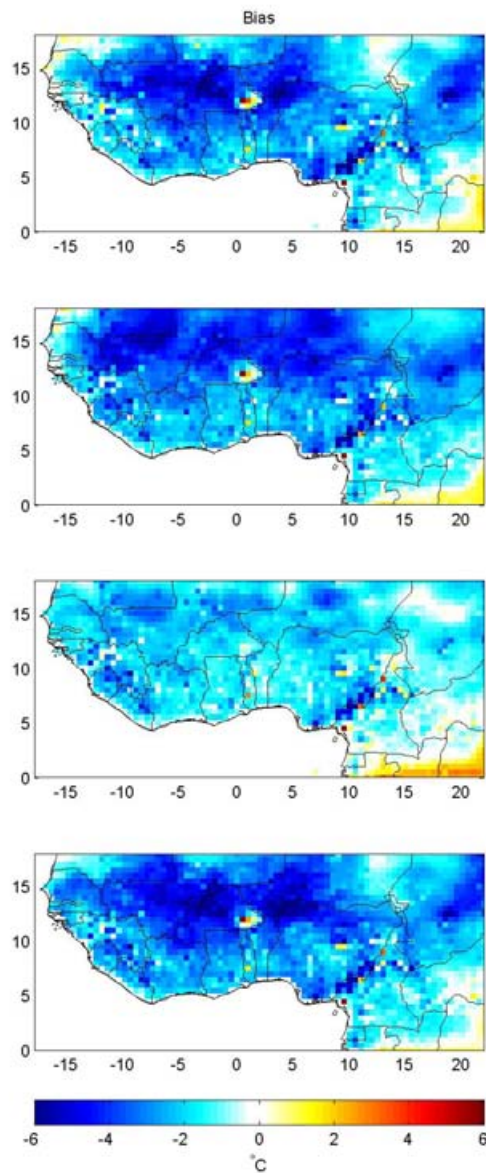


Figure 4.3: The seasonal mean bias of the 2-m air temperature for the historical simulation of EC-EARTH-HIRHAM compared to the UDEL data for 1986-2005.

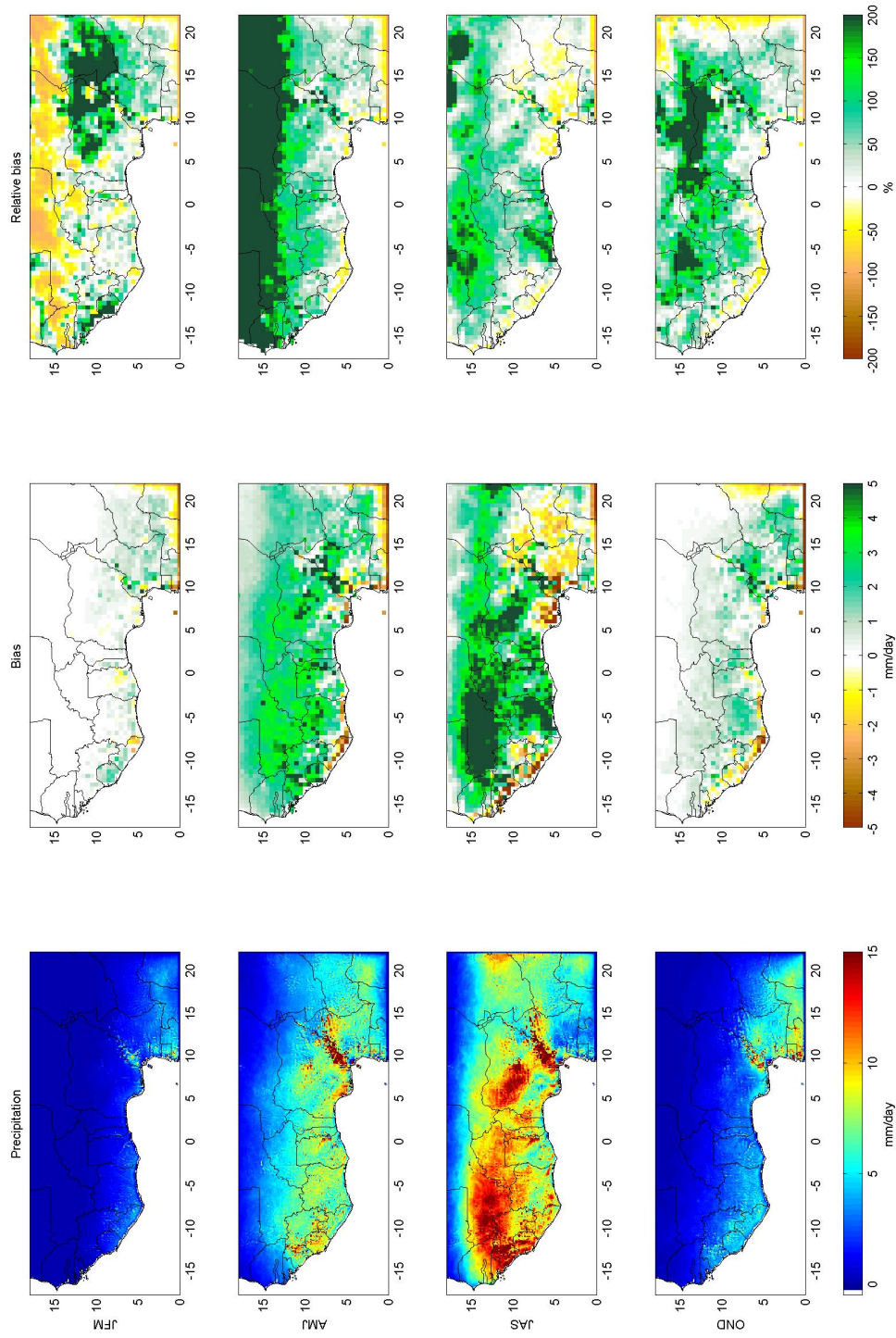


Figure 4.4: Left column shows the seasonal mean precipitation of EC-EARTH-HIRHAM5 historical simulation from 1986-2005 for the four seasons; the middle column shows the seasonal mean bias of the precipitation compared to the UDEL dataset and the right column the relative bias.

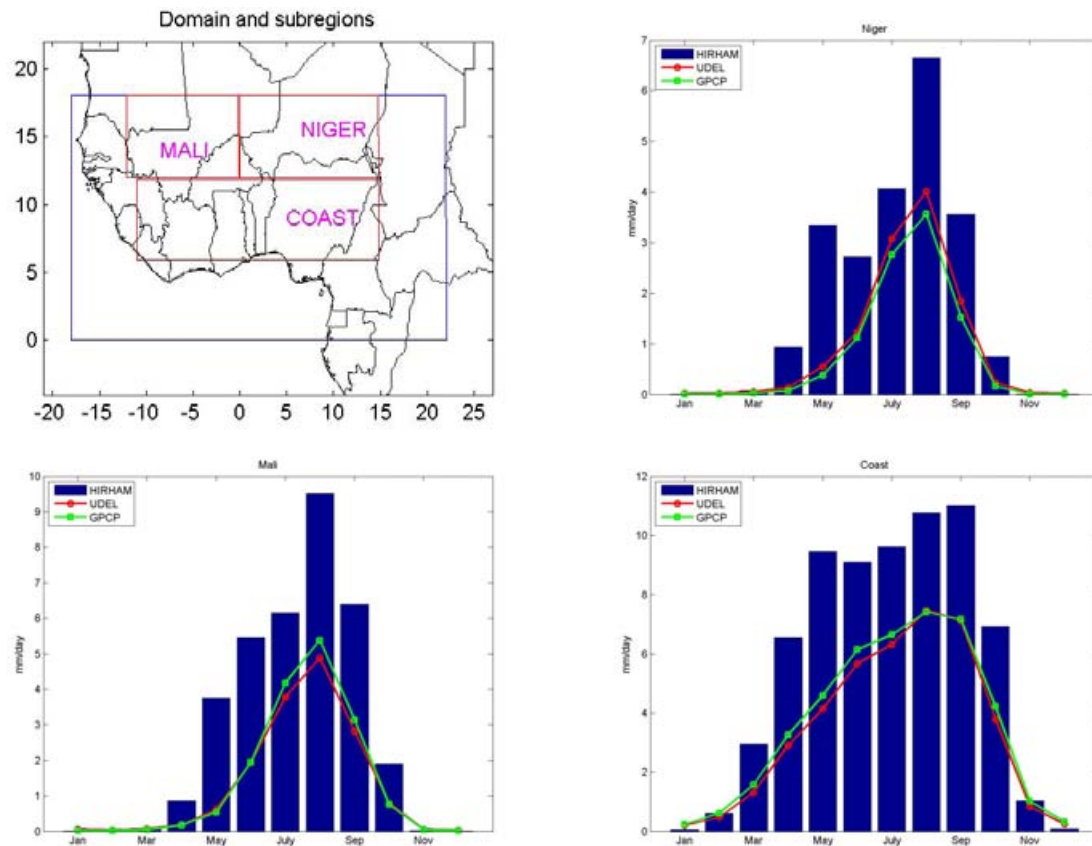


Figure 4.5: Monthly mean precipitation for three different subregions, one centered over Niger, one centered over Mali and one along the coast; the map in the upper left shows the three subregions (in red) and the entire domain (in blue). All values are means over regions and time (1986-2005). The monthly mean precipitation of ECEARTH-HIRHAM5 is here compared to both UDEL and GPCP data.

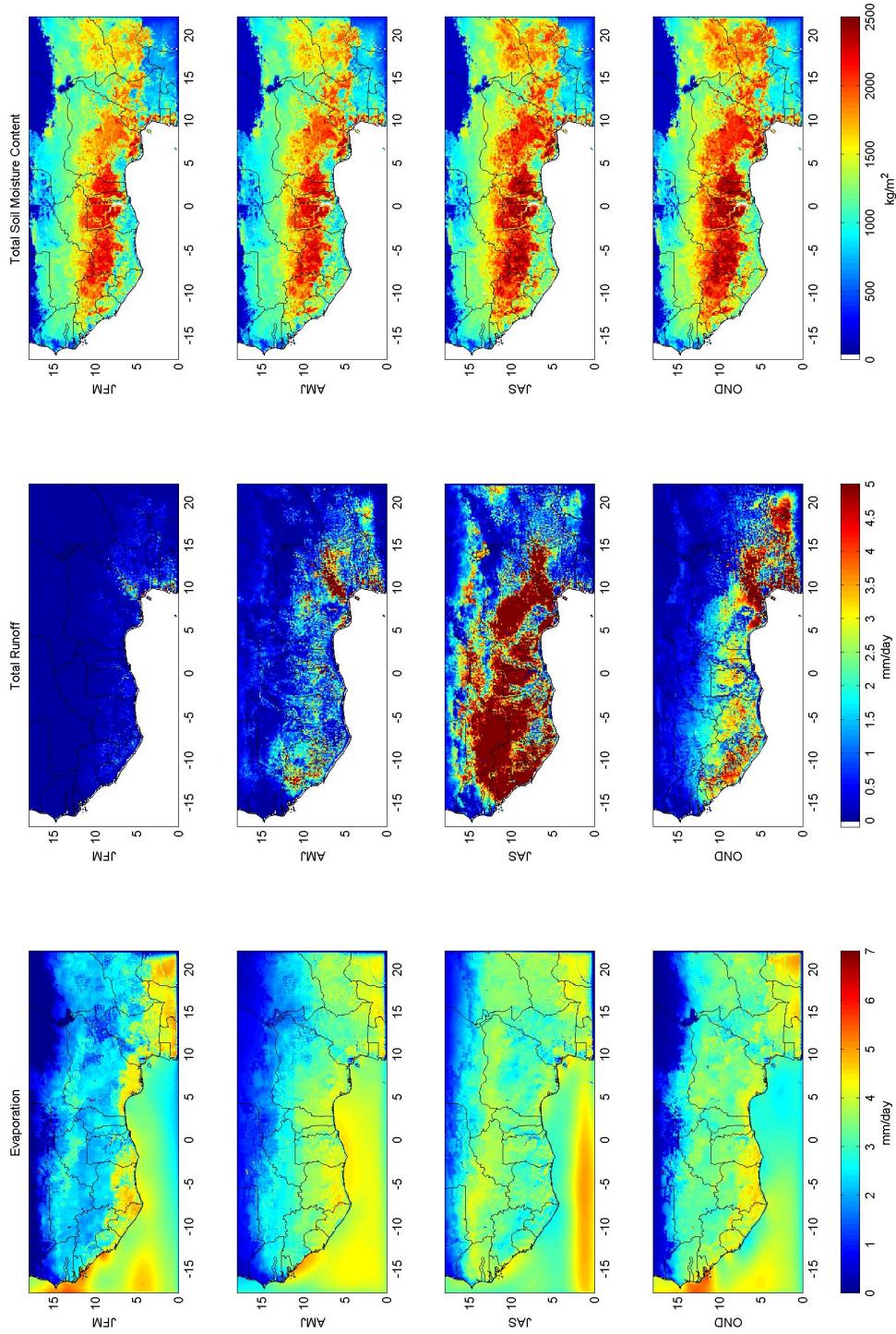


Figure 4.6: The left column shows the seasonal mean evaporation (mm/day), the middle column the total runoff (mm/day), and the right column the seasonal mean soil moisture content (kg/m²) of historical simulation from 1986-2005.

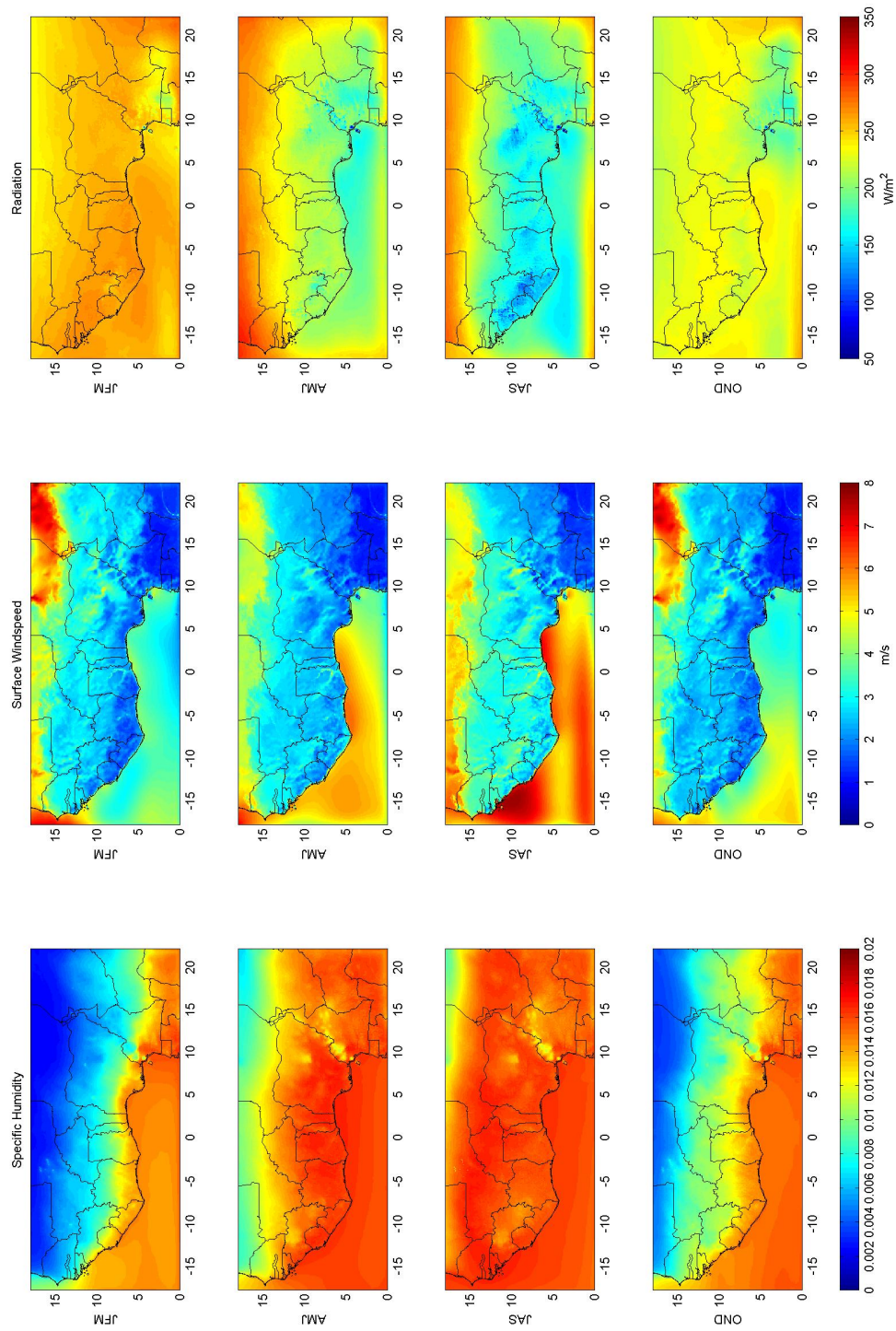


Figure 4.7: Left column shows the seasonal mean specific humidity of the EC-EARTH - HIRHAM5 historical simulation from 1986-2005; the middle column shows the seasonal mean surface wind speed at 10-m (m/s) and the right column the shortwave downwelling radiation at the surface (W/m²).

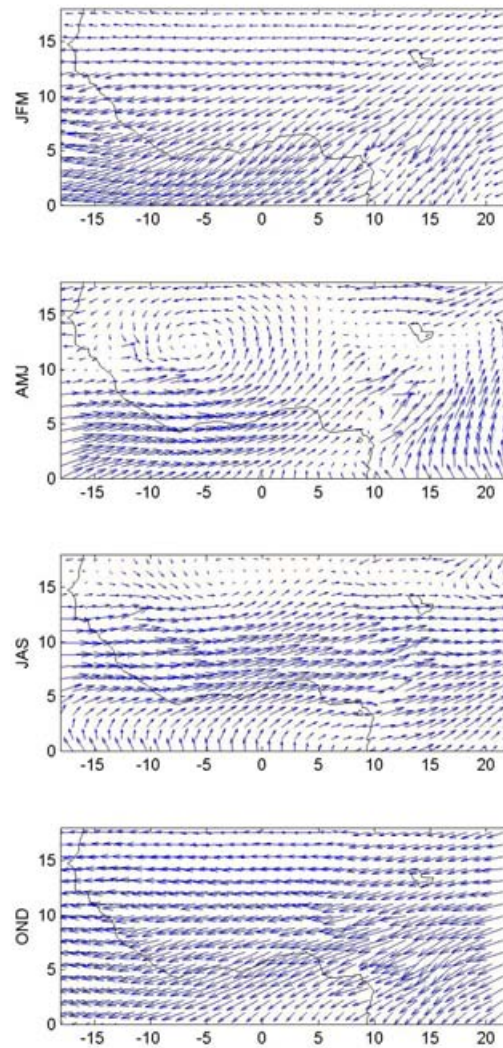


Figure 4.8: Seasonal means of the horizontal moisture flux, $q \cdot \vec{v}$, at 850hPa for the historical simulations of EC-EARTH - HIRHAM5 for the period 1986-2005.

5. Future scenario simulations

To look at the projected climate changes over the region, we have looked at two different scenarios, RCP4.5 and RCP8.5. EC-EARTH has been used to force HIRHAM for both of these scenarios for three different timeslices, 2016-2035, 2046-2065 and 2081-2100. All results in this chapter are presented as climate change maps, i.e. the difference between the future timeslice and the historical timeslice (1986-2005).

Figures 5.1 and 5.2 show the predicted changes in mean temperature for the RCP4.5 and RCP8.5 scenario, respectively, for each of the three future timeslices compared to the historical timeslice. We find that towards the end of the century temperatures will have increased 1-3 K according to RCP4.5 and 3-6 K for RCP8.5. Seasonal differences in temperature increases are small but AMJ is predicted to warm slightly more than the other seasons.

Figures 5.3 and 5.4 show the predicted changes in daily maximum temperature for RCP4.5 and RCP8.5, respectively, and Figures 5.5 and 5.6 the predicted changes in daily minimum temperature. The changes in minimum and maximum temperature are very similar to the

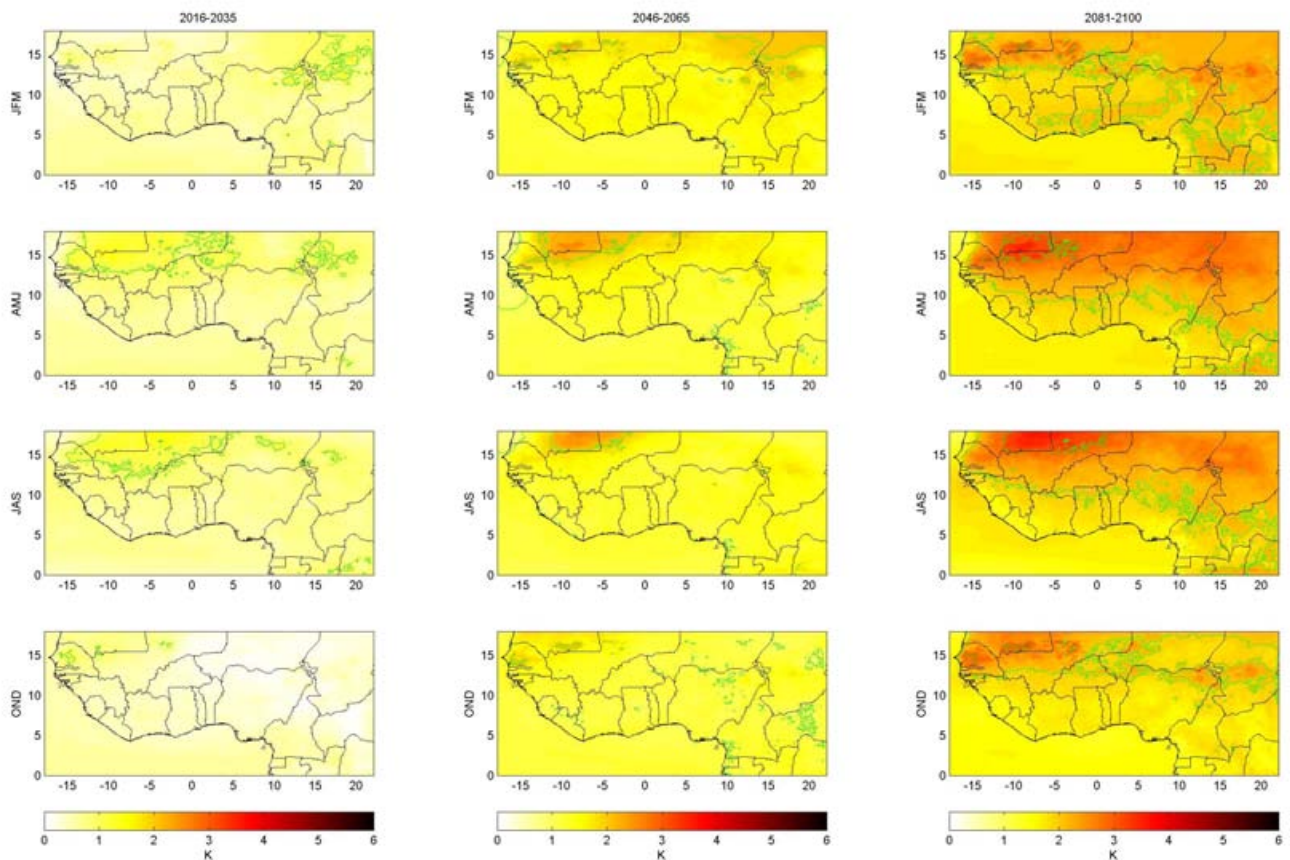


Figure 5.1: The predicted changes in seasonal mean temperature for the RCP4.5 scenario for EC-EARTH-HIRHAM5 for 2016-2035 (left), 2046-2065 (middle) and 2081-2100 (right) compared to the historical time-slice (1986-2005). Green contours are drawn for 1, 2, 3, 4 and 5 K.

changes in mean temperature.

The predicted change in seasonal mean precipitation is shown in Figure 5.7 for RCP4.5 and in Figure 5.8 for RCP8.5. The relative precipitation change is not calculated in areas in which the seasonal mean precipitation in the historical period is less than 0.05 mm/day.

EC-EARTH-HIRHAM predicts a wettening in AMJ from about 0-10°N and from 5-12°N in JAS and drying north of this, particularly in the western part of the domain. Changes are stronger in RCP8.5 than in RCP4.5 with positive changes of 20-30% in RCP8.5.

Figure 5.9 shows predicted changes in seasonal mean evaporation for RCP4.5 and Figure 5.10 the same for RCP8.5. The geographical pattern of the changes in evaporation reflects the changes in precipitation; as expected evaporation increases where precipitation increases and vice versa, but the area of increased evaporation extends further north than the area of increased precipitation in both AMJ and JAS.

Figures 5.11 and 5.12 show the predicted changes in seasonal mean specific humidity for RCP4.5 and RCP8.5, respectively. The specific humidity is predicted to increase in both scenarios particularly towards the end of the century with increases exceeding 40% in large parts of the domain in AMJ in RCP8.5.

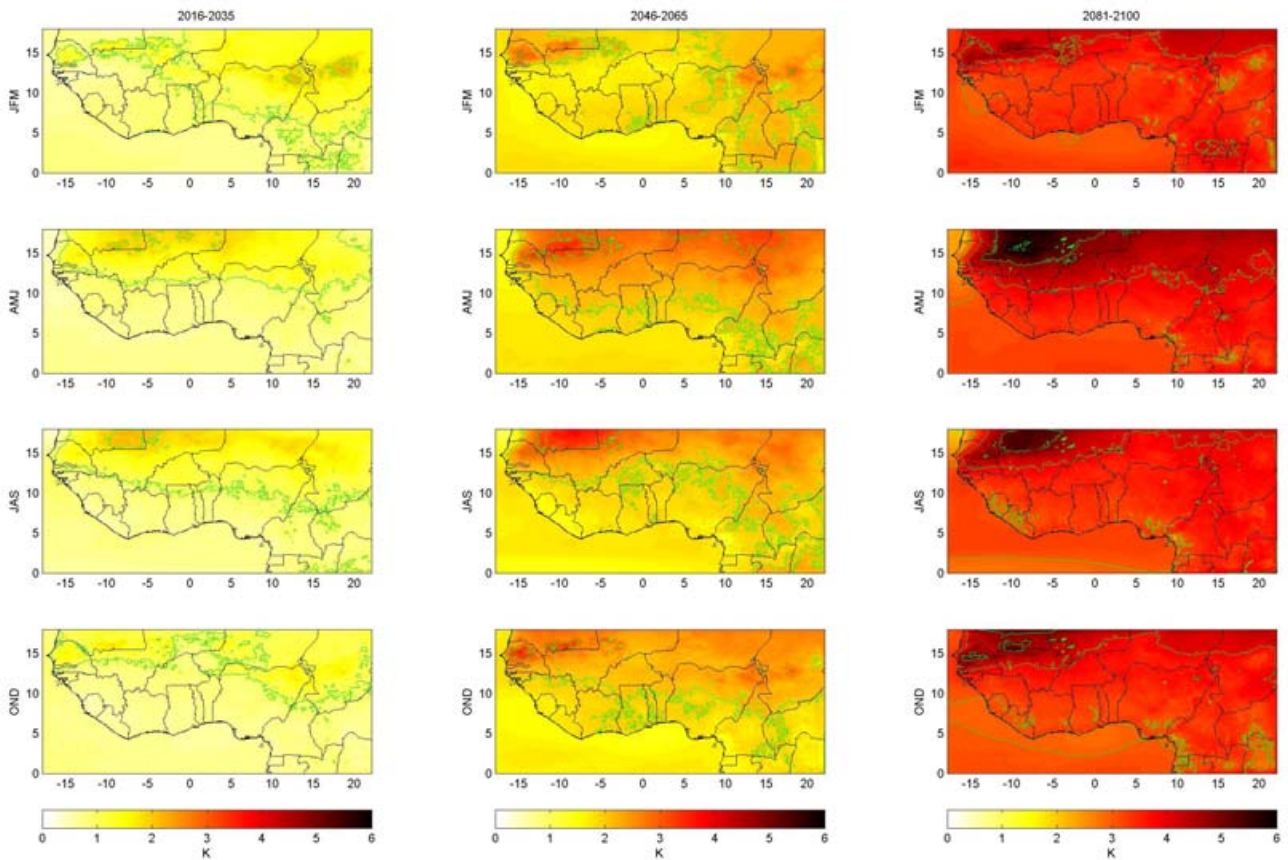


Figure 5.2: The predicted changes in seasonal mean temperature for the RCP8.5 scenario for EC-EARTH-HIRHAM5 for 2016-2035 (left), 2046-2065 (middle) and 2081-2100 (right) compared to the historical time-slice (1986-2005). Green contours are drawn for 1, 2, 3, 4 and 5 K.

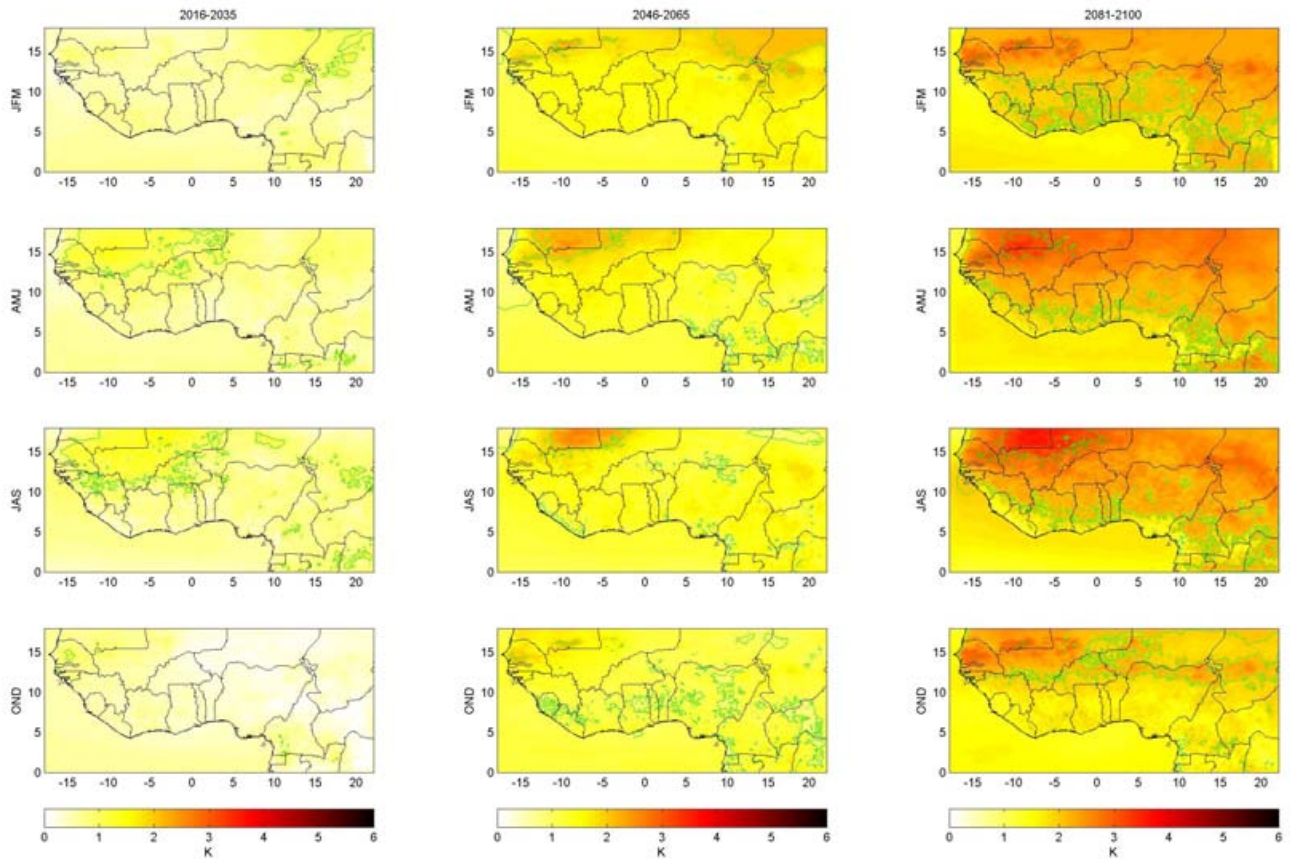


Figure 5.3: Predicted changes in seasonal mean maximum temperature for the RCP4.5 scenario for EC-EARTH-HIRHAM5 for 2016-2035 (left), 2046-2065 (middle) and 2081-2100 (right) compared to the historical time-slice (1986-2005). Green contours are drawn for 1, 2, 3, 4 and 5 K.

Figures 5.13 and 5.14 show the predicted changes in the total runoff for RCP4.5 and RCP8.5, respectively. The changes in runoff are characterized by small scale features, but with some general patterns of increasing runoff along the southwest coast and decreasing runoff in the Sahel.

Figures 5.15 and 5.16 show the predicted changes in seasonal mean 10-m wind speed for RCP4.5 and RCP8.5, respectively. Figures 5.17 and 5.18 show the predicted changes in the shortwave downwelling radiation. In both scenarios the shortwave downwelling radiation increases towards the end of the century in all seasons except OND, where it decreases.

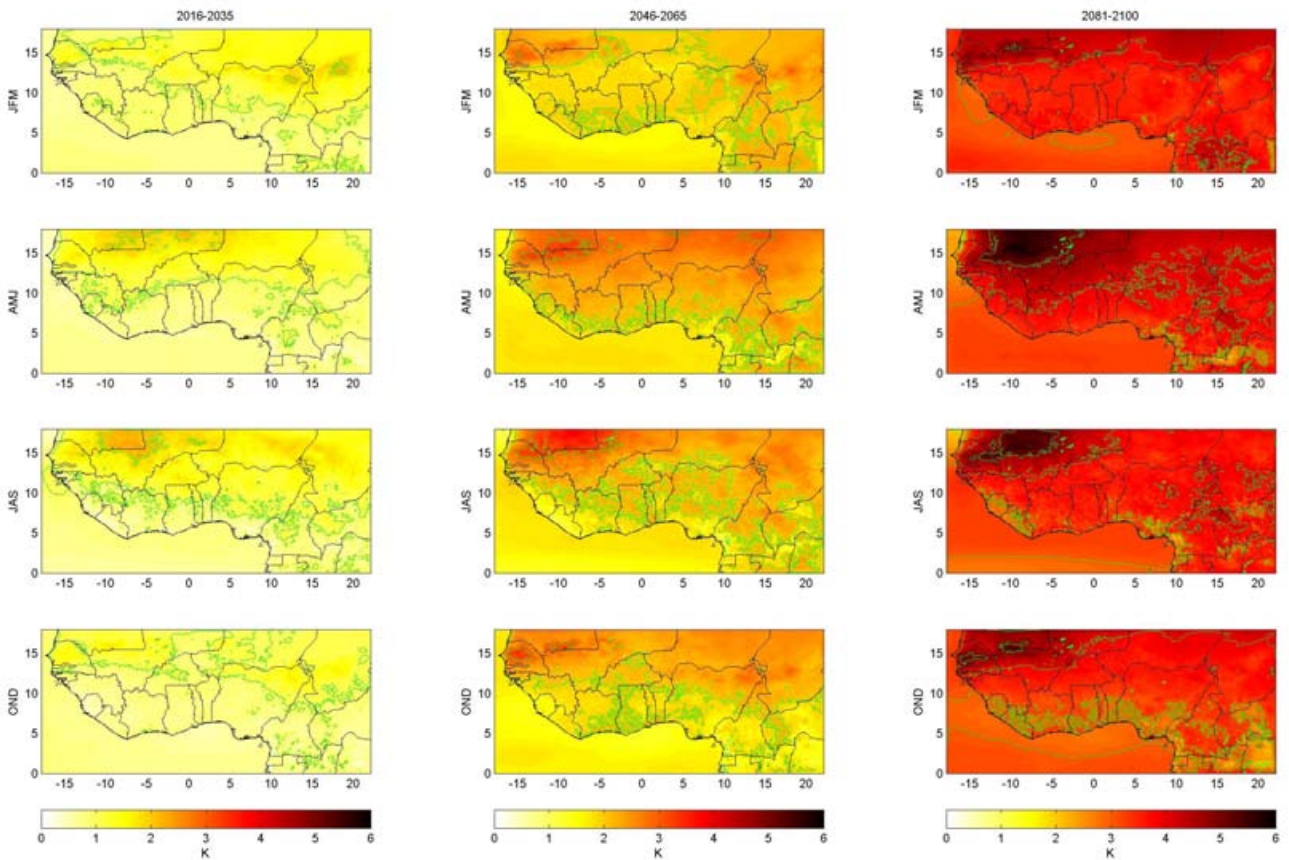


Figure 5.4: Predicted changes in seasonal mean maximum temperature for the RCP8.5 scenario for EC-EARTH-HIRHAM5 for 2016-2035 (left), 2046-2065 (middle) and 2081-2100 (right) compared to the historical time-slice (1986-2005). Green contours are drawn for 1, 2, 3, 4 and 5 K.

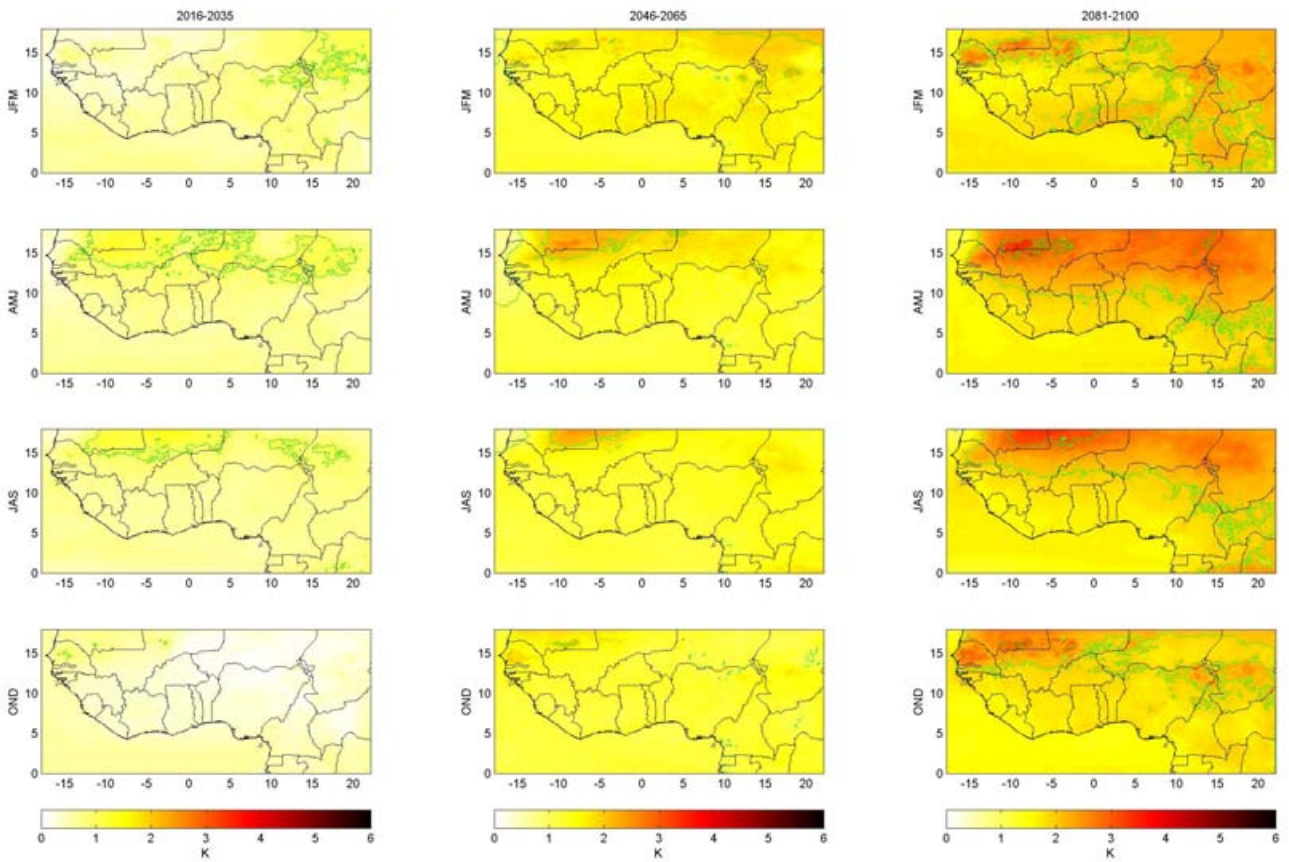


Figure 5.5: Predicted changes in seasonal mean minimum temperature for the RCP4.5 scenario for EC-EARTH-HIRHAM5 for 2016-2035 (left), 2046-2065 (middle) and 2081-2100 (right) compared to the historical time-slice (1986-2005). Green contours are drawn for 1, 2, 3, 4 and 5 K.

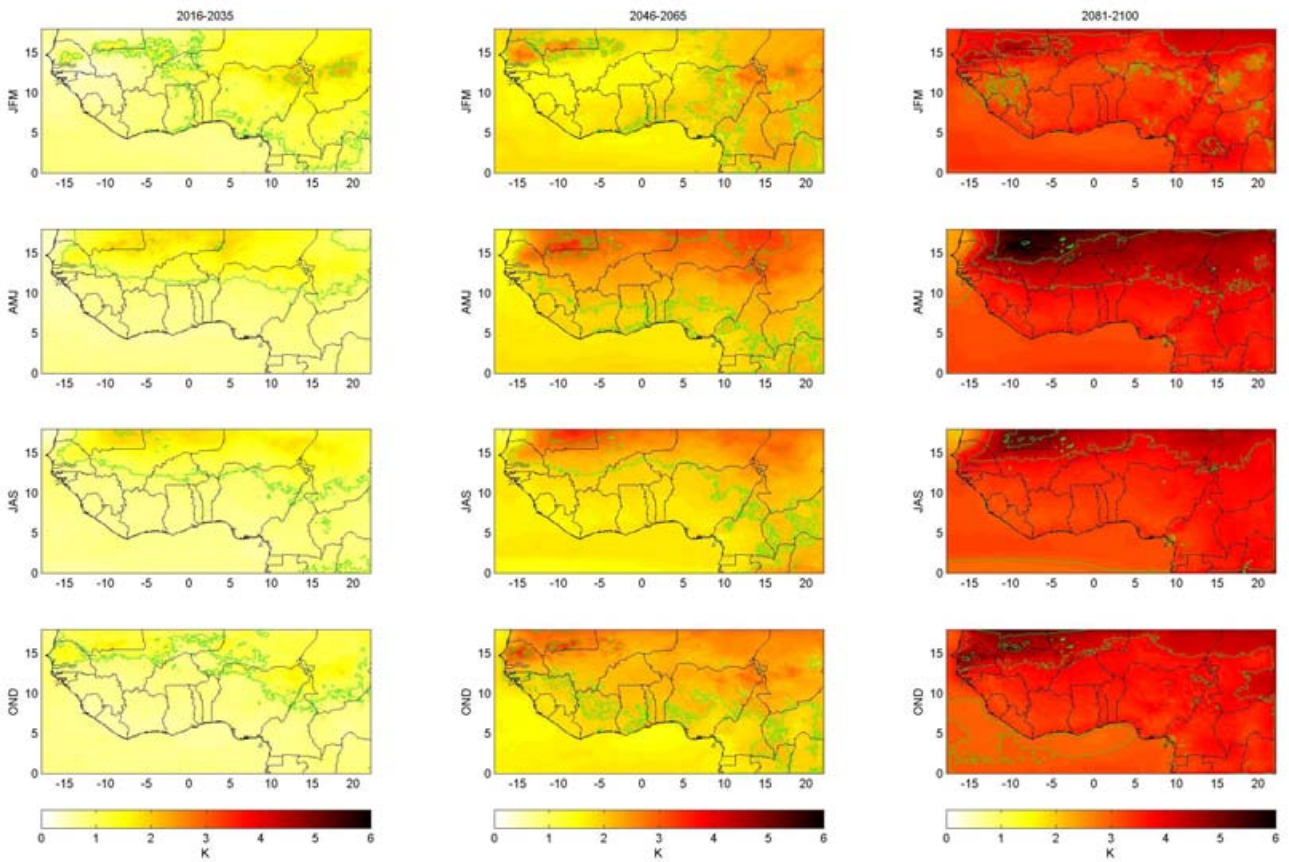


Figure 5.6: Predicted changes in seasonal mean minimum temperature for the RCP8.5 scenario for EC-EARTH-HIRHAM5 for 2016-2035 (left), 2046-2065 (middle) and 2081-2100 (right) compared to the historical time-slice (1986-2005). Green contours are drawn for 1, 2, 3, 4 and 5 K.

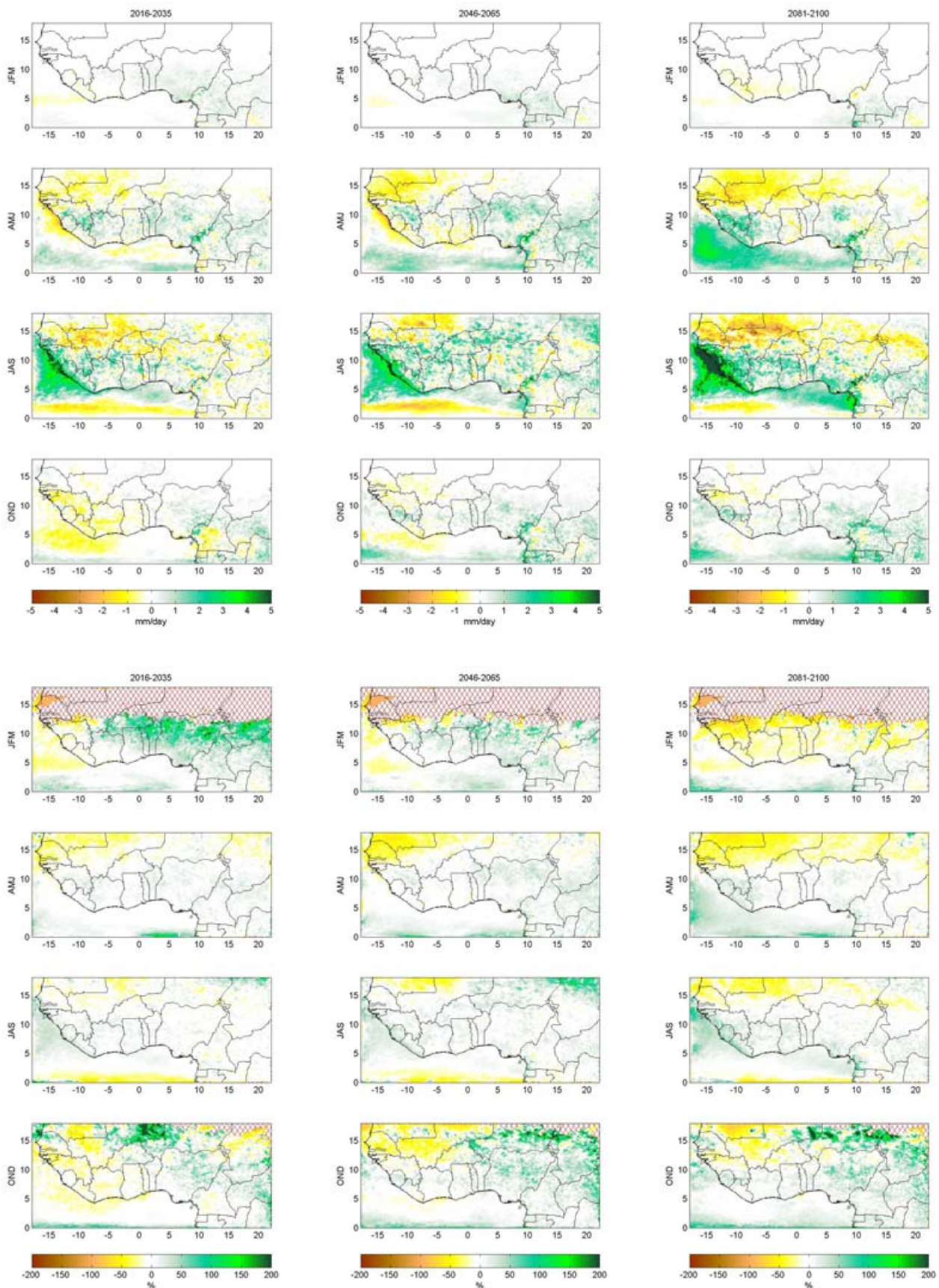


Figure 5.7: Predicted changes in seasonal mean precipitation for the RCP4.5 scenario for EC-EARTH-HIRHAM5 for 2016-2035 (left), 2046-2065 (middle) and 2081-2100 (right) compared to the historical time-slice (1986-2005).

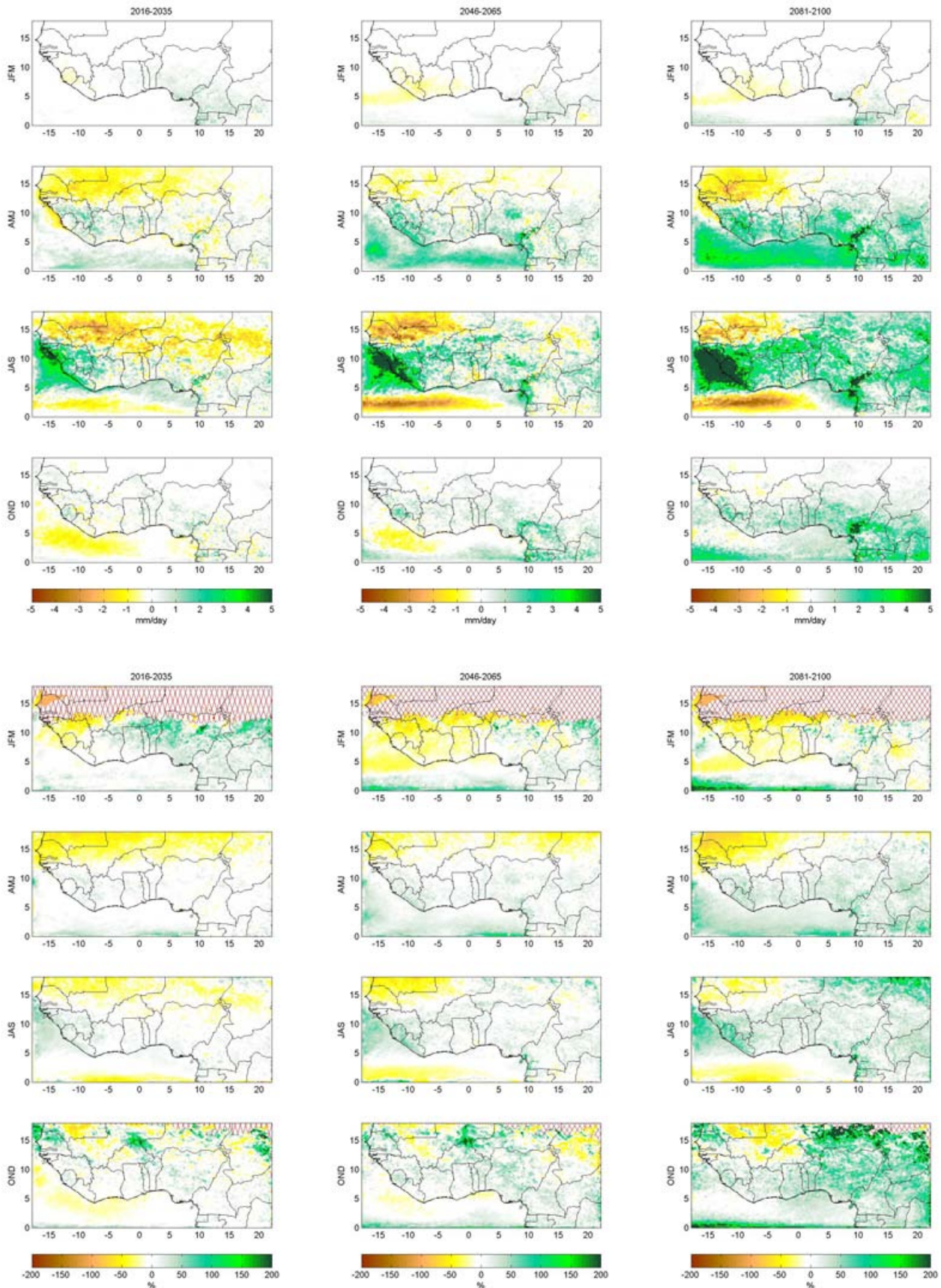


Figure 5.8: Predicted changes in seasonal mean precipitation for the RCP8.5 scenario for EC-EARTH-HIRHAM5 for 2016-2035 (left), 2046-2065 (middle) and 2081-2100 (right) compared to the historical time-slice (1986-2005).

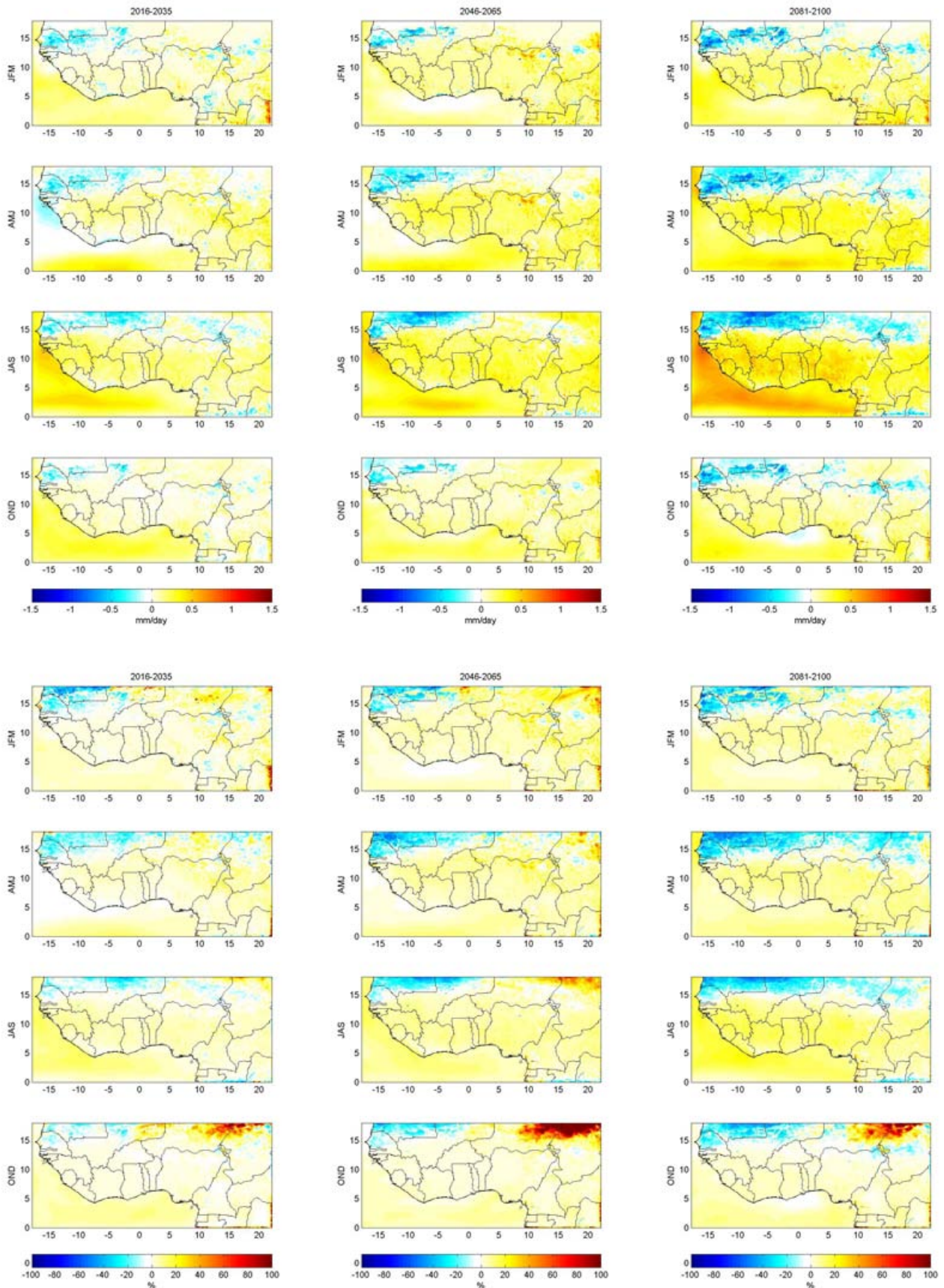


Figure 5.9: Predicted changes in seasonal mean evaporation for the RCP4.5 scenario for EC-EARTH-HIRHAM5 for 2016-2035 (left), 2046-2065 (middle) and 2081-2100 (right) compared to the historical time-slice (1986-2005).

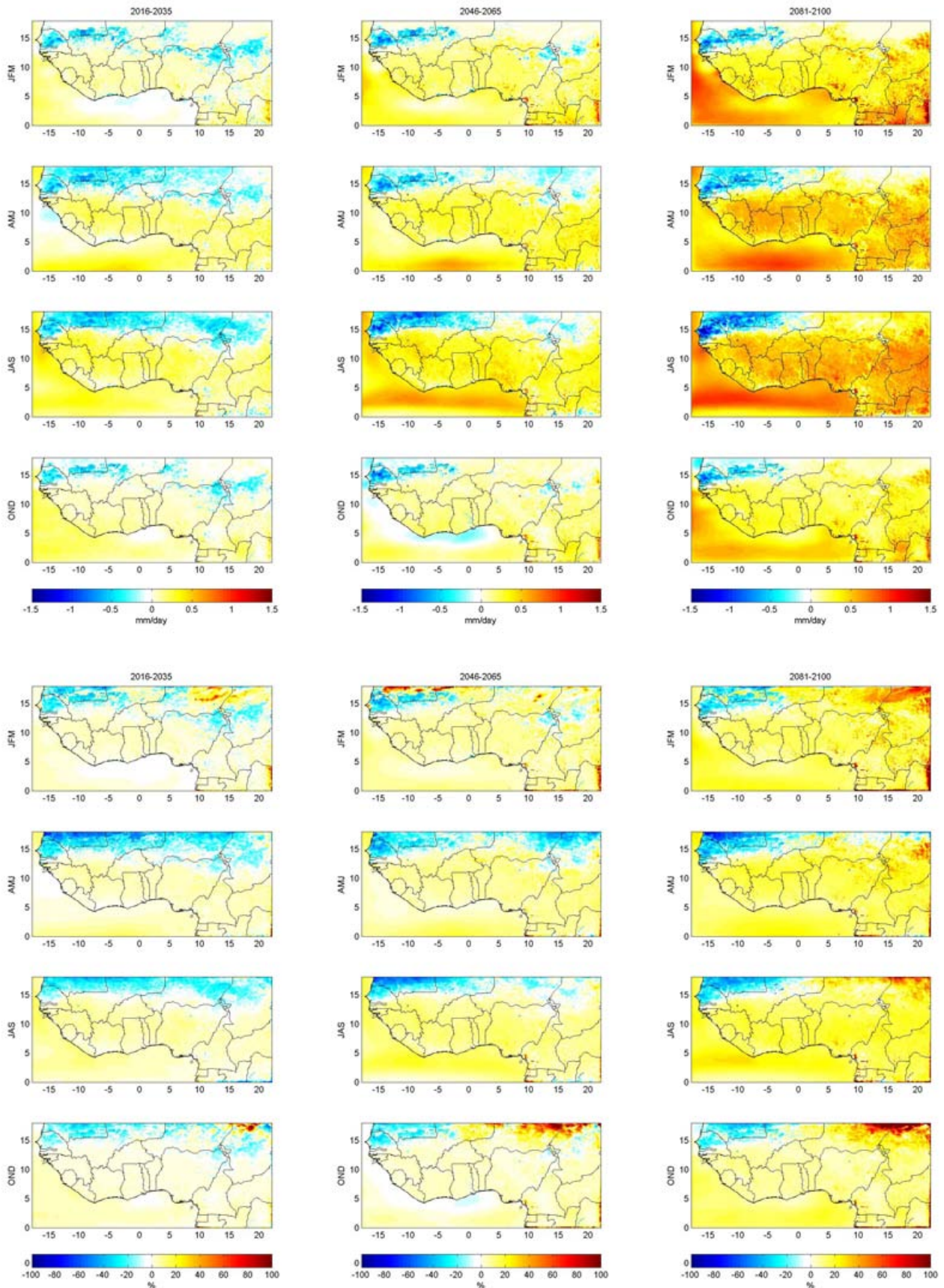


Figure 5.10: Predicted changes in seasonal mean evaporation for the RCP8.5 scenario for EC-EARTH-HIRHAM5 for 2016-2035 (left), 2046-2065 (middle) and 2081-2100 (right) compared to the historical time-slice (1986-2005).

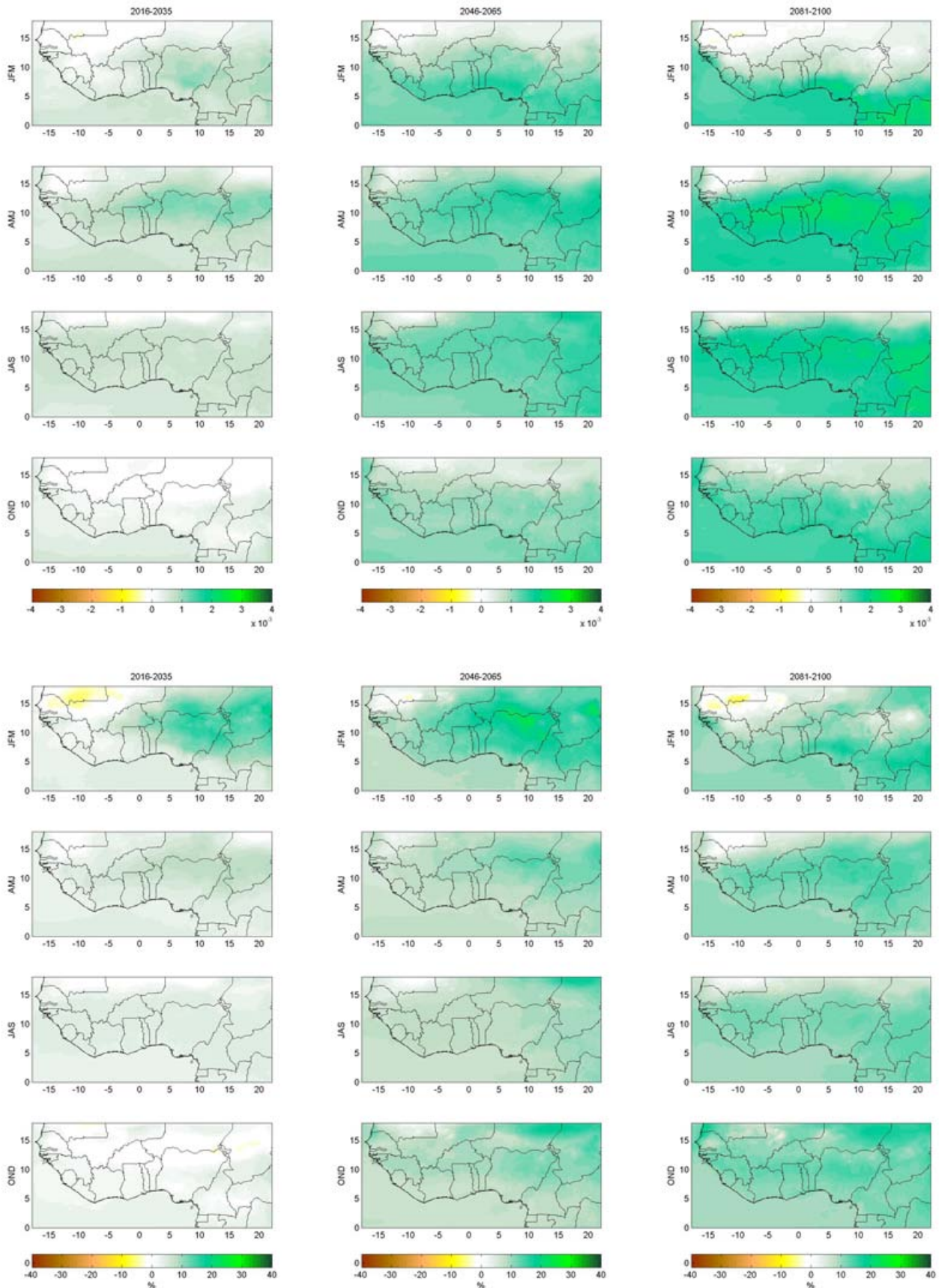


Figure 5.11: Predicted changes in seasonal mean specific humidity for the RCP4.5 scenario for EC-EARTH-HIRHAM5 for 2016-2035 (left), 2046-2065 (middle) and 2081-2100 (right) compared to the historical time-slice (1986-2005).

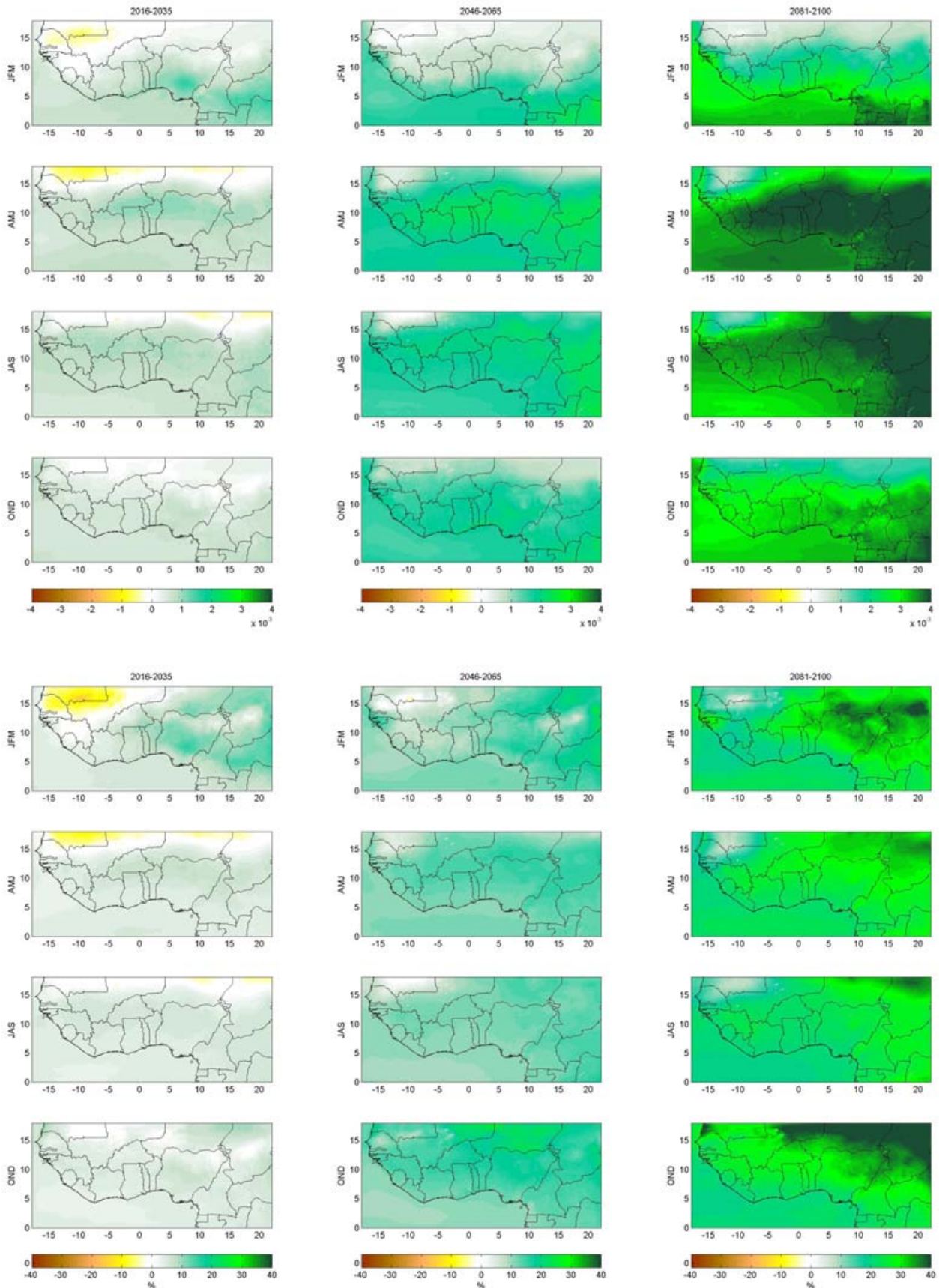


Figure 5.12: Predicted changes in seasonal mean specific humidity for the RCP8.5 scenario for EC-EARTH-HIRHAM5 for 2016-2035 (left), 2046-2065 (middle) and 2081-2100 (right) compared to the historical time-slice (1986-2005).

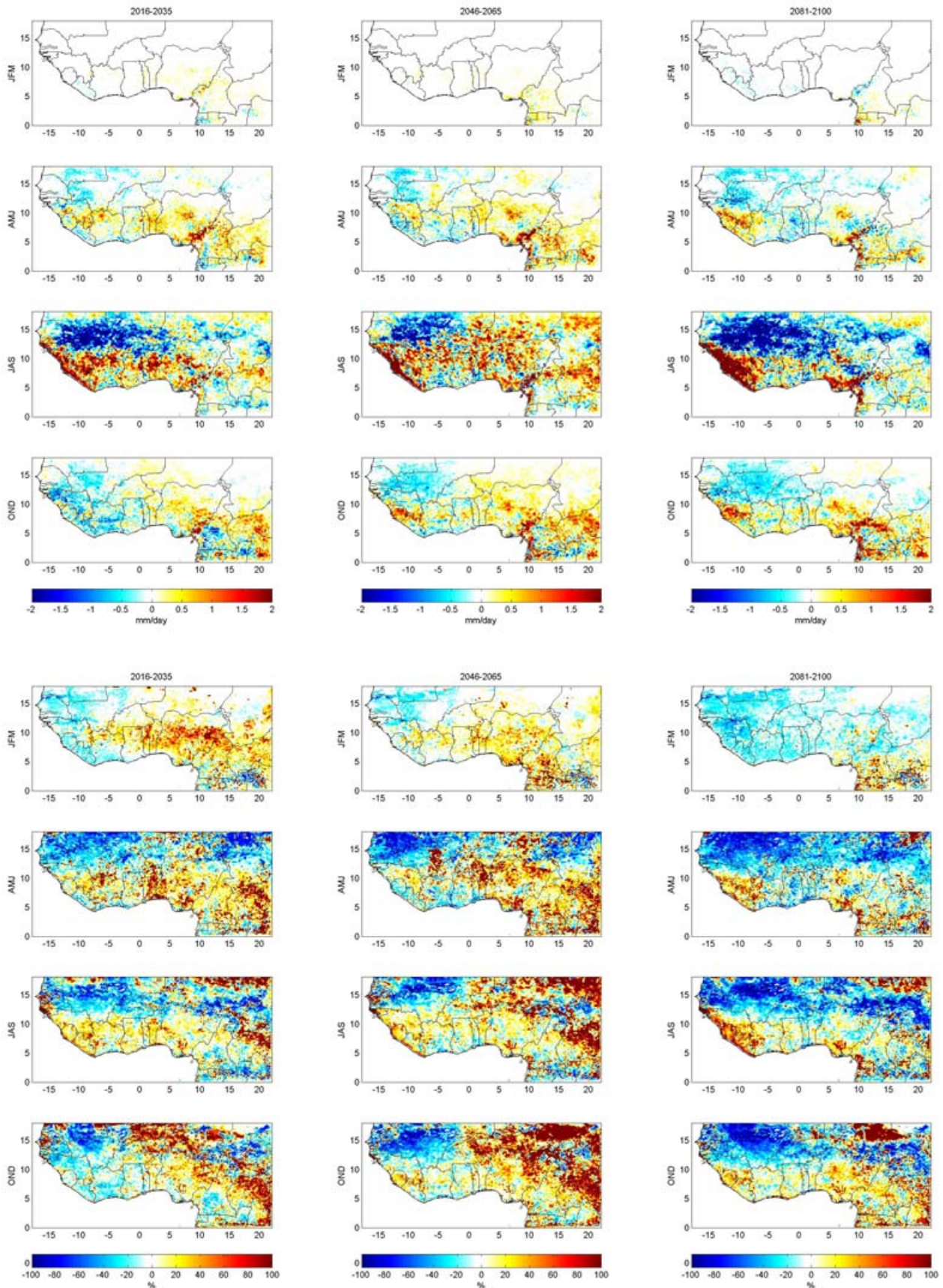


Figure 5.13: Predicted changes in seasonal mean total runoff for the RCP4.5 scenario for EC-EARTH-HIRHAM5 for 2016-2035 (left), 2046-2065 (middle) and 2081-2100 (right) compared to the historical time-slice (1986-2005).

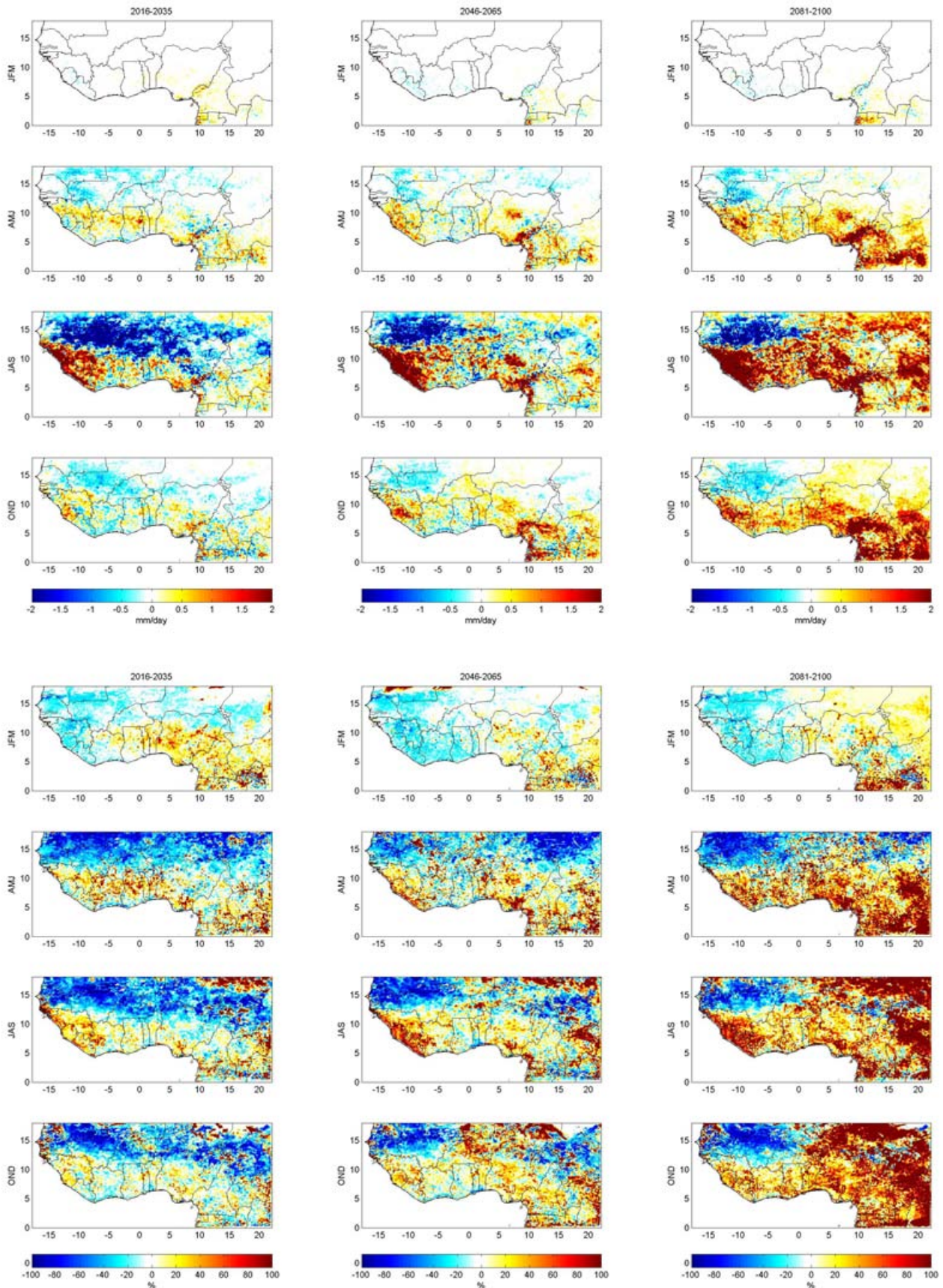


Figure 5.14: Predicted changes in seasonal mean total runoff for the RCP8.5 scenario for EC-EARTH-HIRHAM5 for 2016-2035 (left), 2046-2065 (middle) and 2081-2100 (right) compared to the historical time-slice (1986-2005).

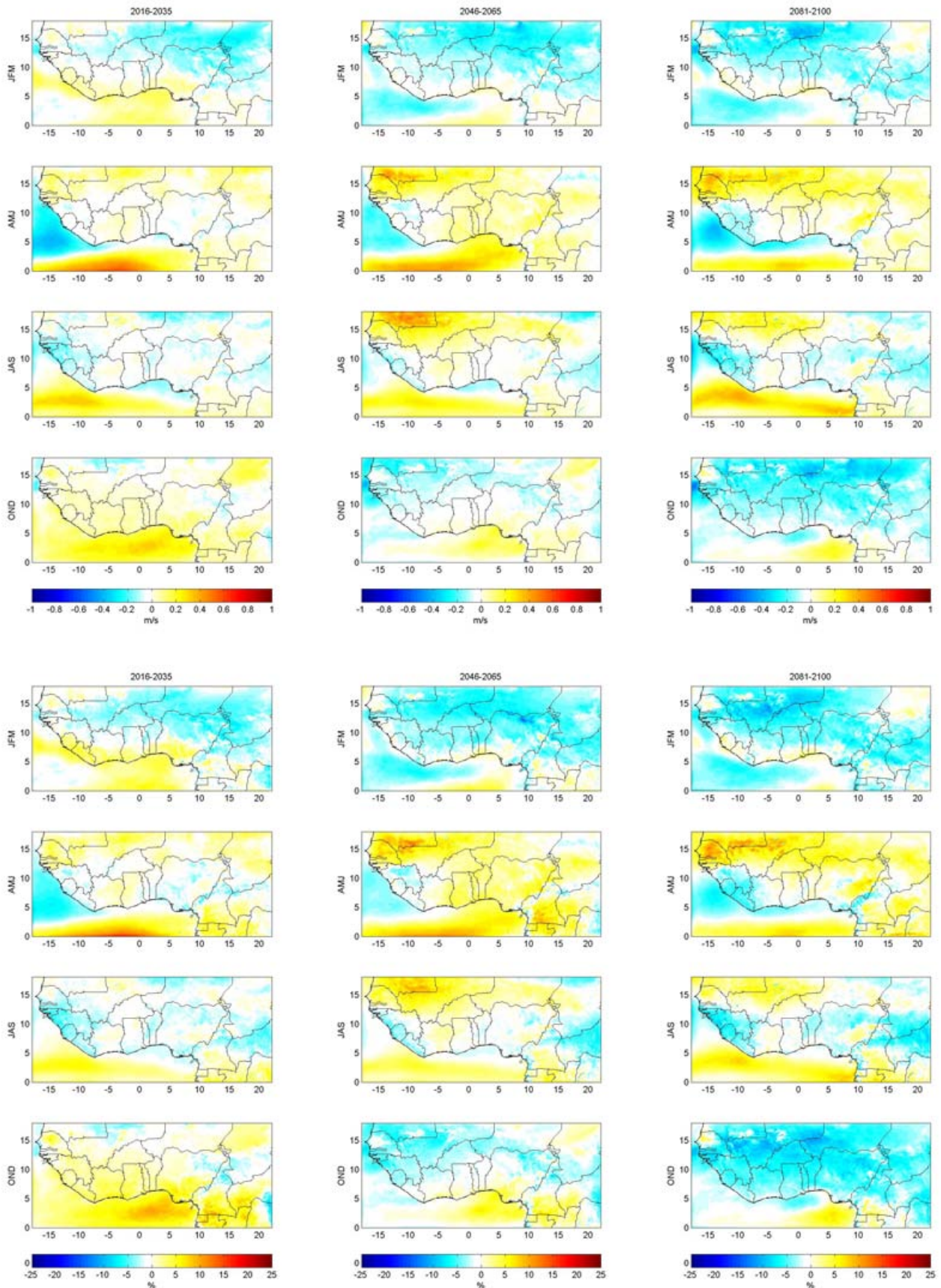


Figure 5.15: Predicted changes in seasonal mean surface wind speed (at 10-m) for the RCP4.5 scenario for EC-EARTH-HIRHAM5 for 2016-2035 (left), 2046-2065 (middle) and 2081-2100 (right) compared to the historical time-slice (1986-2005).

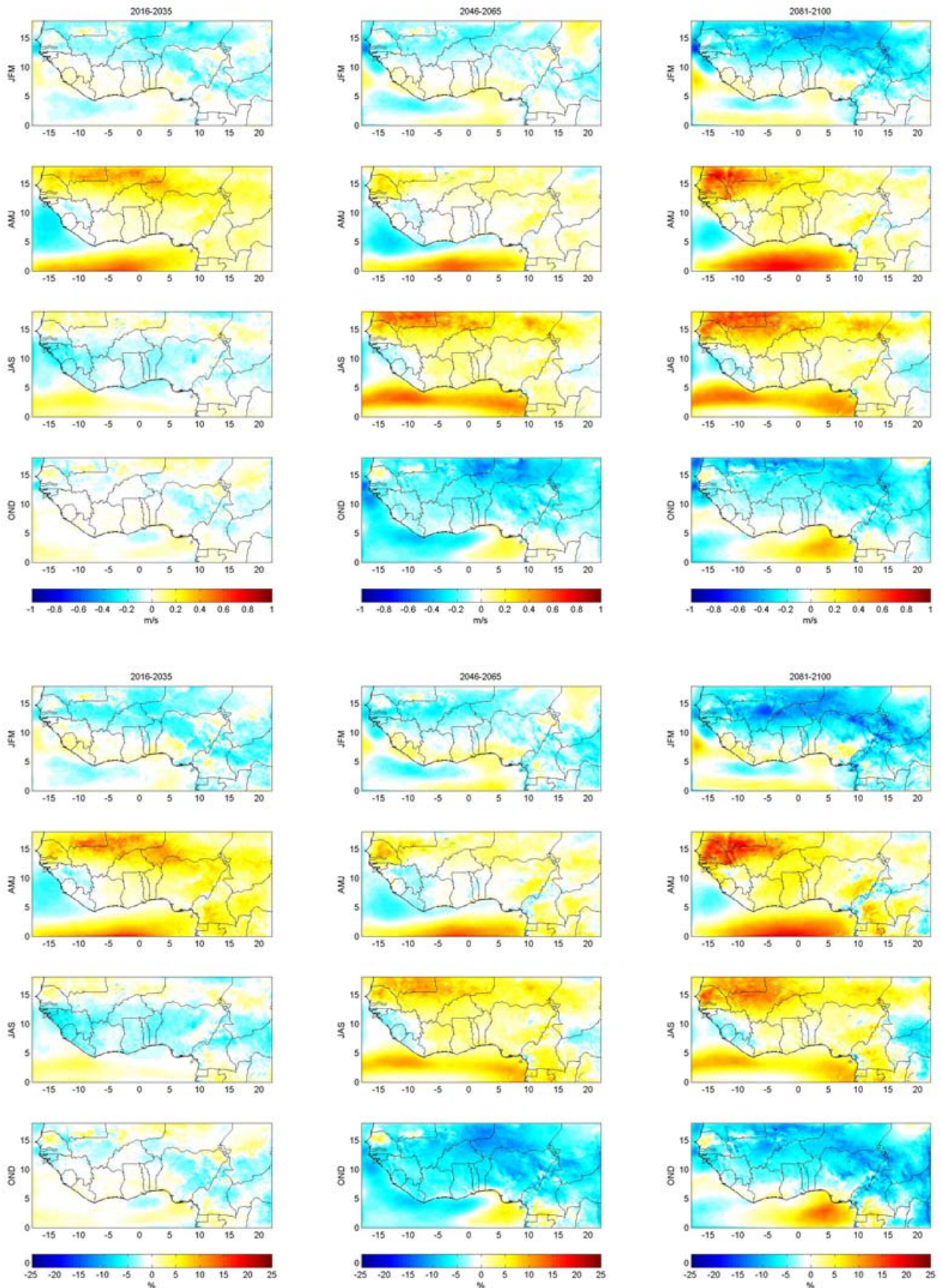


Figure 5.16: Predicted changes in seasonal mean surface wind speed (at 10-m) for the RCP8.5 scenario for EC-EARTH-HIRHAM5 for 2016-2035 (left), 2046-2065 (middle) and 2081-2100 (right) compared to the historical time-slice (1986-2005).

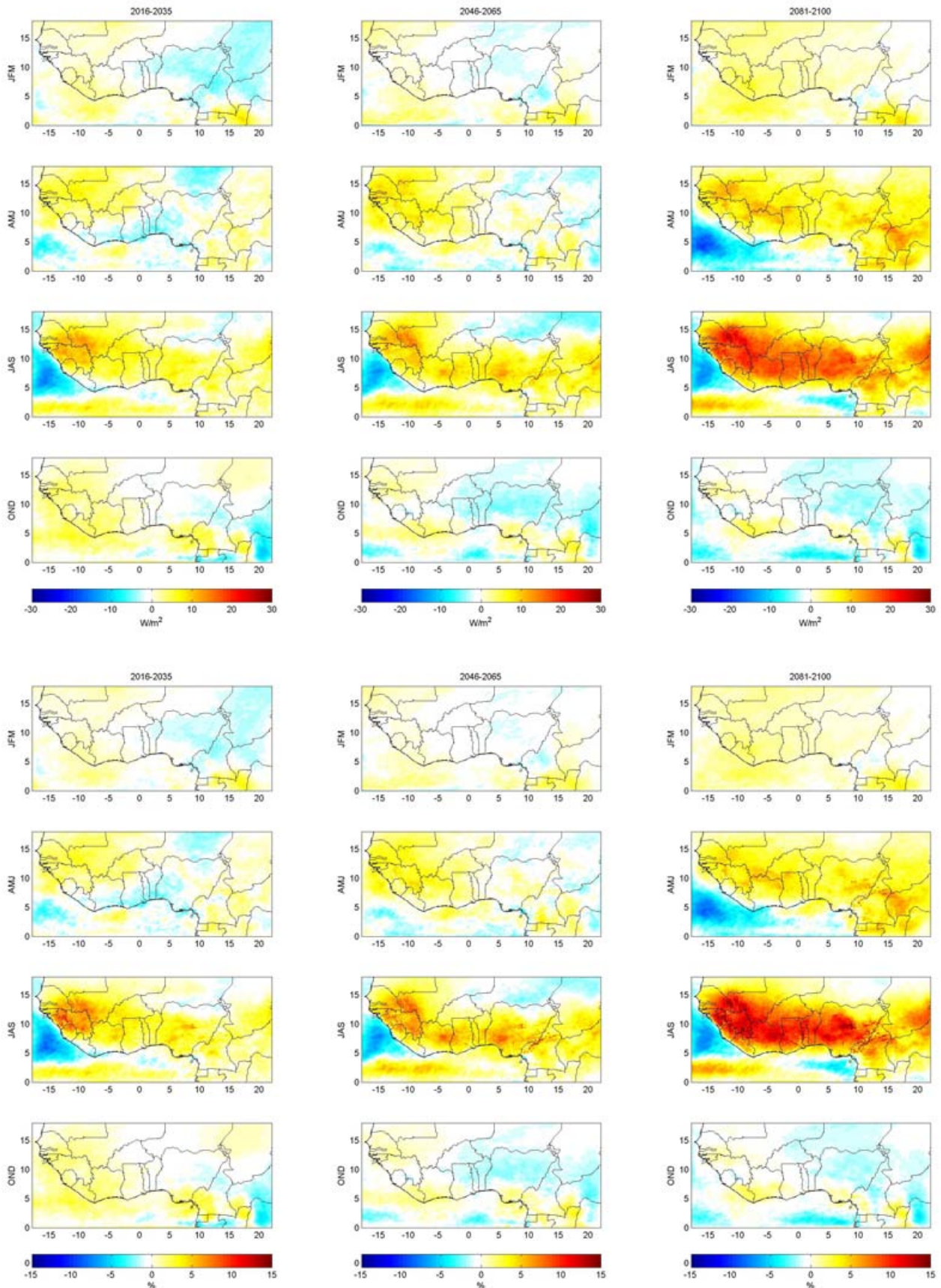


Figure 5.17: Predicted changes in seasonal mean shortwave downwelling radiation at the surface for the RCP4.5 scenario for EC-EARTH-HIRHAM5 for 2016-2035 (left), 2046-2065 (middle) and 2081-2100 (right) compared to the historical time-slice (1986-2005).

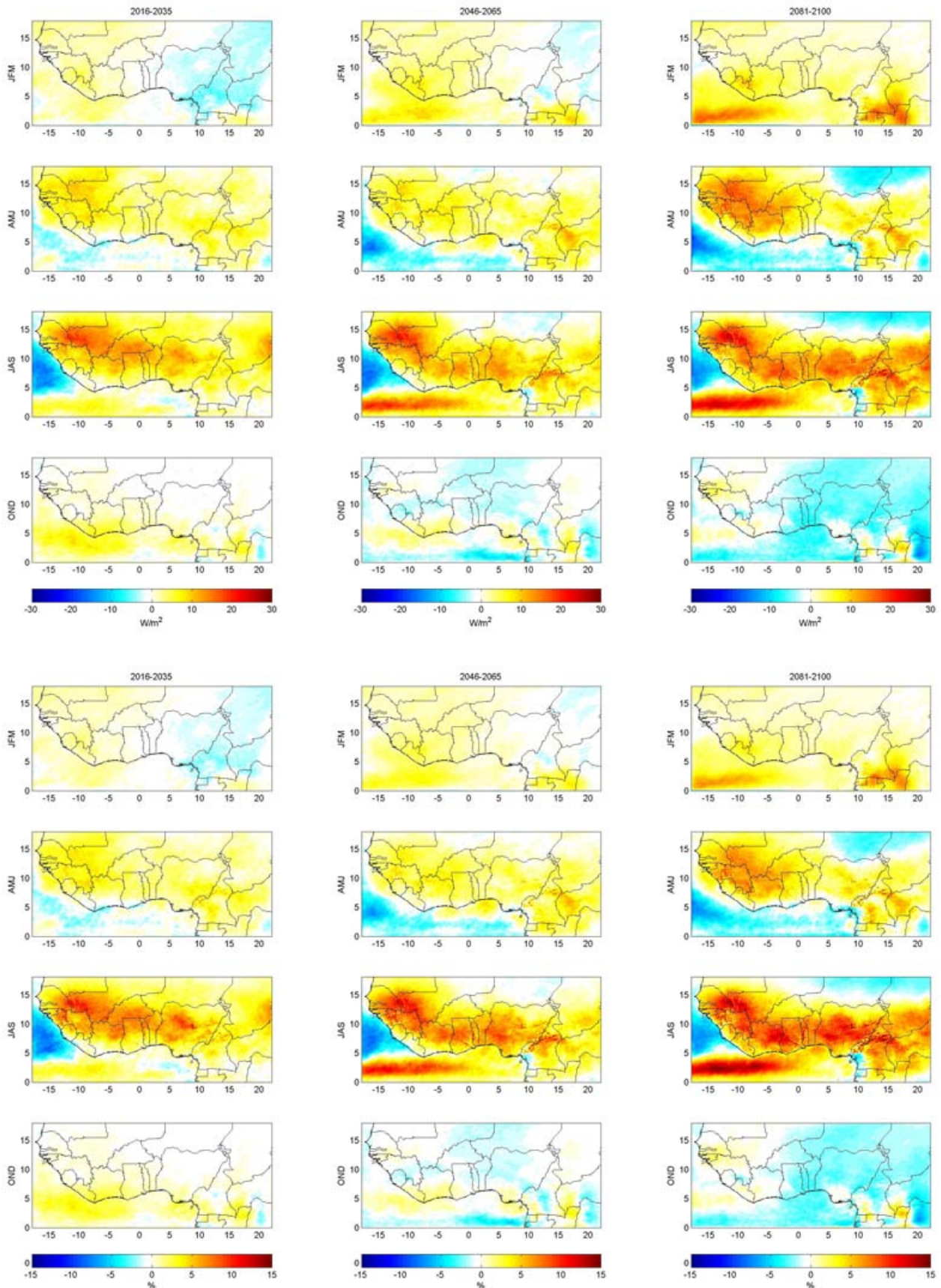


Figure 5.18: Predicted changes in seasonal mean shortwave downwelling radiation at the surface for the RCP8.5 scenario for EC-EARTH-HIRHAM5 for 2016-2035 (left), 2046-2065 (middle) and 2081-2100 (right) compared to the historical time-slice (1986-2005).

A. Grid specifications

Specifications of the grid without relaxation zones

deg = 0.11

POLON = N/A

POLAT = 90.00

Nlon = 366

Nlat = 165

WEST = -18.04

EAST = 22.11

SOUTH = 0.00

NORTH = 18.04

References

- Christensen, O.B., Drews, M., Christensen, J.H., Dethloff, K., Ketelsen, K., Hebestadt, I., & Rinke, A., 2006. The HIRHAM regional climate model version 5 (β). DMI Technical Report 06-17, <http://www.dmi.dk/fileadmin/Rapporter/TR/tr06-17.pdf>.
- Christensen, O.B., Gutowski, W.J., Nikulin, G. & Legutke, S. 2013. CORDEX Archive Design, version 3.0, December 2013.
http://cordex.dmi.dk/joomla/images/CORDEX/cordex_archive_specifications.pdf
- Dee, D.P., Uppala, S.M., Simmons, A.J., Berrisford, P., Poli, P., Kobayashi, S., Andrae, U., Balmaseda, G., Balsamo, G., Bauer, P., Bechtold, P., Beljaars, A.C.M., van de Berg, L., Bidlot, J., Bormann, N., Delsol, C., Dragani, R., Fuentes, M., Geer, A.J., Haimberger, L., Healy, S.B., Hersbach, H., Hólm, E.V., Isaksen, I., Kållberg, P., Köhler, M., Matricardi, M., McNally, A.P., Monge-Sanz, B.M., Morcrette, J.-J., Park, B.-K., Peubey, C., de Rosnay, P., Tavolato, C., Thépaut, N., & Vitart, F., 2011. The ERA-Interim reanalysis: configuration and performance of the data assimilation system, *Quarterly journal of the Royal Meteorological Society*, **137**, 656, 553-597.
- Eerola, K., 2013. Twenty-one years of verification from the HIRLAM NWP system, *Wea. Forecasting*, **28**, 270-285, doi: 10.1175/WAF-D-12-00068.1.
- Hazeleger, W., Wang, X., Severijns, C., Ștefănescu, S., Bintanja, R., Sterl, A., Wyser, K., Semmler, T., Yang, S., van den Hurk, B., van Noije, T., van der Linden, E., & K. van der Wiel, 2012. EC-Earth V2.2: description and validation of a new seamless Earth system prediction model. *Clim Dyn.*, **39**, 2611-2629, doi: 10.1007/s00382-011-1228-5.
- Legates, D.R., & Willmott, C.J., 1990. Mean seasonal and spatial variability in gauge-corrected, global precipitation. *Int. J. Climatol.*, **10**, 111-127.
- Matsuura, K., & Willmott, C.J., 2012a. Terrestrial Air Temperature: 1900-2010 Gridded Monthly Time Series, http://climate.geog.udel.edu/~climate/html_pages/Global2011/...README.GlobalTsT2011.html.
- Matsuura, K., & Willmott, C.J., 2012b. Terrestrial precipitation: 1900-2010 Gridded Monthly Time Series, http://climate.geog.udel.edu/~climate/html_pages/Global2011/...Precip_revised_3.02/README.GlobalTsP2011.html.
- Nikulin, G., Jones, C., Giorgi, F., Asrar, G., Buchner, M., Cerezo-Mota, R., Christensen O.B., Deque, M., Fernandez, J., Hansler, A., Meijgaard, E.V., Samuelsson, P., Sylla, M.B. & Sushama, L., 2012. Precipitation climatology in an Ensemble of CORDEX-Africa Regional Climate Simulations, *J. Clim.*, **25**, 6057-6078.
- Roeckner, E., Bäuml, G., Bonaventura, L., Brokopf, R., Esch, M., Giorgetta, M., et al., 2003. The atmospheric general circulation model ECHAM 5. PART I: Model description.
- Uppala, S., Kållberg, P., Simmons, A., Andrae, U., Da Costa Bechtold, V., Fiorino, M., Gibson, J., Haseler, J., Hernandez, A., Kelly, G., Li, X., Onogi, K., Saarinen, S., Sokka, N., Allan, R., Andersson, E., Arpe, K., Balmaseda, M., Beljaars, A., Van De Berg, L., Bidlot, J., Bormann, N., Caires, S., Chevallier, F., Dethof, A., Dragosavac, M., Fisher, M., Fuentes,



Danish Meteorological Institute
Scientific Report 15-01

M., Hagemann, S., Hólm, E., Hoskins, B., Isaksen, L., Janssen, P., Jenne, R., McNally, A., Mahfouf, J., Morcrette, J., Rayner, N., Saunders, R., Simon, P., Sterl, A., Trenberth, K., Untch, A., Vasiljevic, D., Viterbo, P., & Woollen, J., 2005. The ERA-40 re-analysis, *Q J R Meteorol Soc*, **131**(612):29613012. doi:10.1256/qj.04.176